Radiation Damage Fundamentals: Primary Damage Production:

Roger E. Stoller

Materials Science and Technology Division

Oak Ridge National Laboratory

Joint EFRC Summer School

Idaho Falls, ID

6 to 10 June 2011

Outline

Illustrate the range of radiation-induced phenomena of concern

Discuss primary radiation damage formation in the form of atomic displacement cascades, focus on molecular dynamics simulation

- some background information on radiation sources
- evolution of atomic displacement cascades
  - time structure, roughly 0 to 0.5 ps, 0.5 to 10 ps, >10 ps
  - subcascade formation
  - in-cascade recombination and stable defect formation
  - in-cascade clustering
- statistical variations in cascade behavior
- effect of primary variables: T, E
- secondary variables: effects of microstructural length scales, surfaces, pre-existing damage
- material differences: bcc vs. fcc vs hcp, metal vs. oxide (e.g. UO2)

Appendix on secondary damage models, dpa, SRIM, damage correlation

Why do we care about radiation damage in materials?

- Desirable material properties: strength, ductility, toughness, dimensional stability, are all largely determined by the nature of their defect structure
  - grain size, other internal interfaces
  - dislocation density
  - size and density of second phase precipitates

- Irradiation with energetic particles leads to atomic displacements
  - neutron exposure can expressed in terms of particle fluence (#/m^2) or a dose unit that accounts for atomic displacements per atom - dpa
  - lifetime component exposures are in the range of ~0.01 to more than 100 dpa
  - cumulative impact of atomic displacements: radiation-induced evolution of pre-existing microstructure and the formation of new defect structure

Incoming particle

Primary knock-on atom - PKA
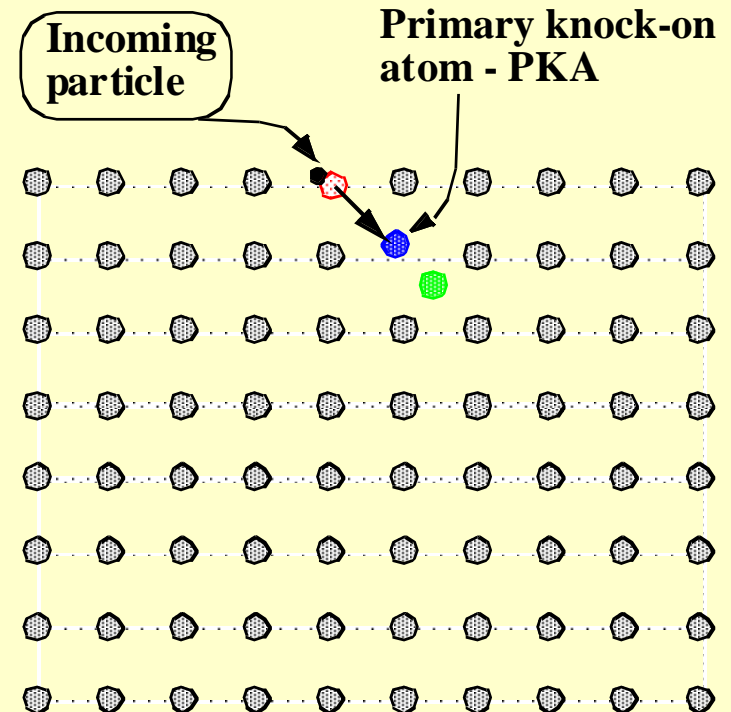
Example: Radiation-induced microstructure in austenitic stainless steel
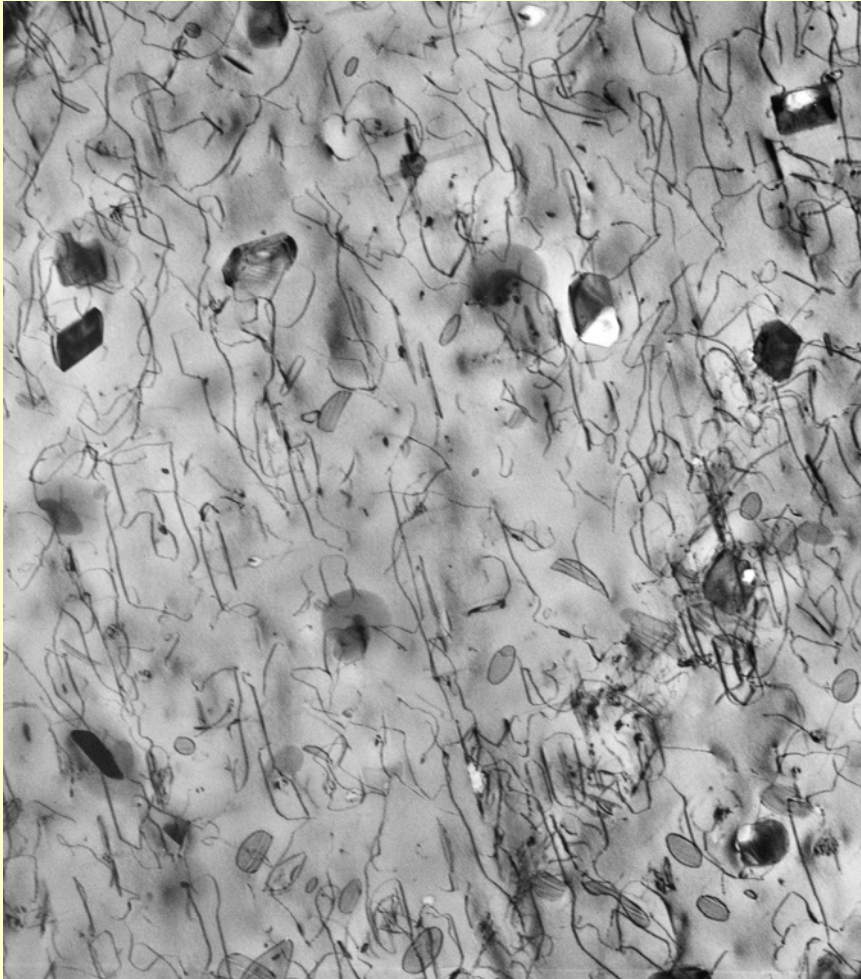
- Frank faulted dislocation loops, network dislocation evolution
- formation of second phase precipitates, some are non-equilibrium
- cavity formation and void swelling

IRRADIATION - INDUCED SWELLING

20% CW 316
633°C

1 cm

UNIRRADIATED CONTROL

1.5×10^{23} n/cm^2 (E>0.1 MeV)

Example: Influence on deformation behavior

- dense defect microstructures at lower temperatures lead to high hardening
- flow localization (dislocation channeling) in ~defect-free channels

Nb

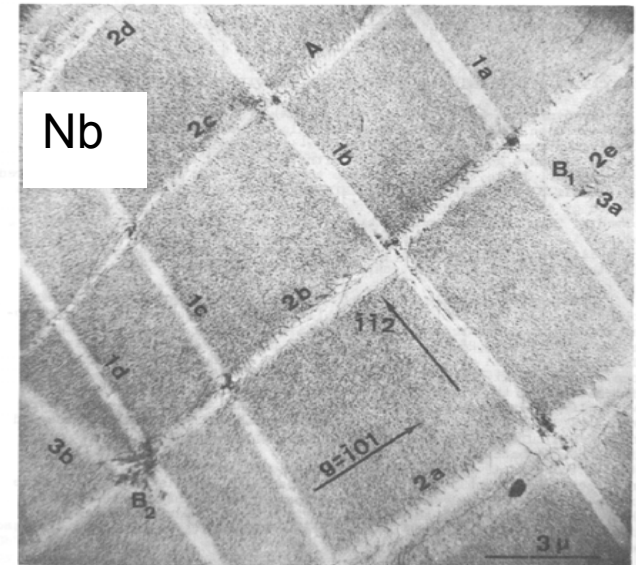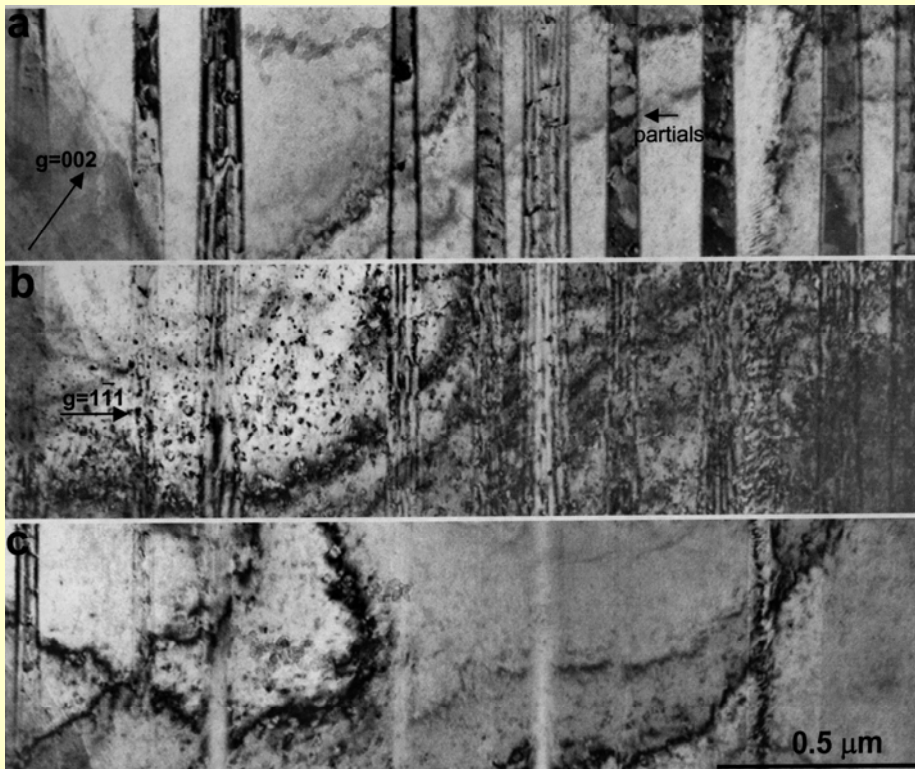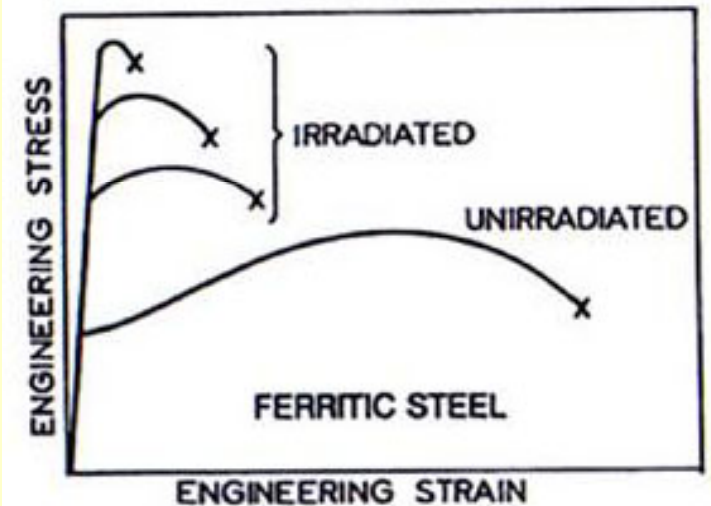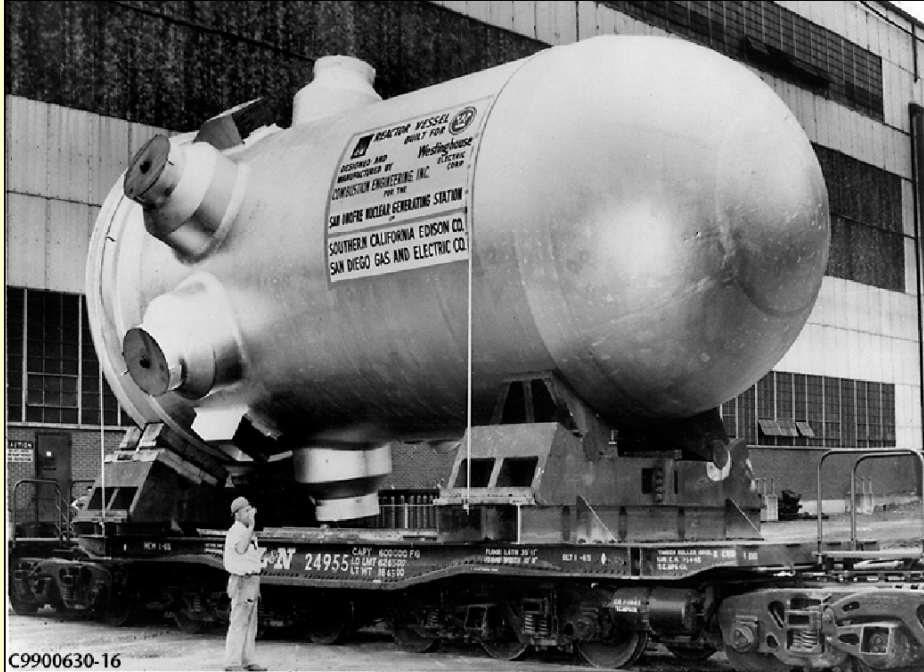FIG. 5. Rectangular pattern of dislocation channels in niobium irradiated to 4.4 × 10^{18} n/cm^2 (E > 1 MeV) at 50°C and strained to 6.0% at room temperature.

Austenitic Stainless steel

g=002

g=111

partials

0.5 μm

ENGINEERING STRESS

IRRADIATED

UNIRRADIATED

FERRITIC STEEL

ENGINEERING STRAIN

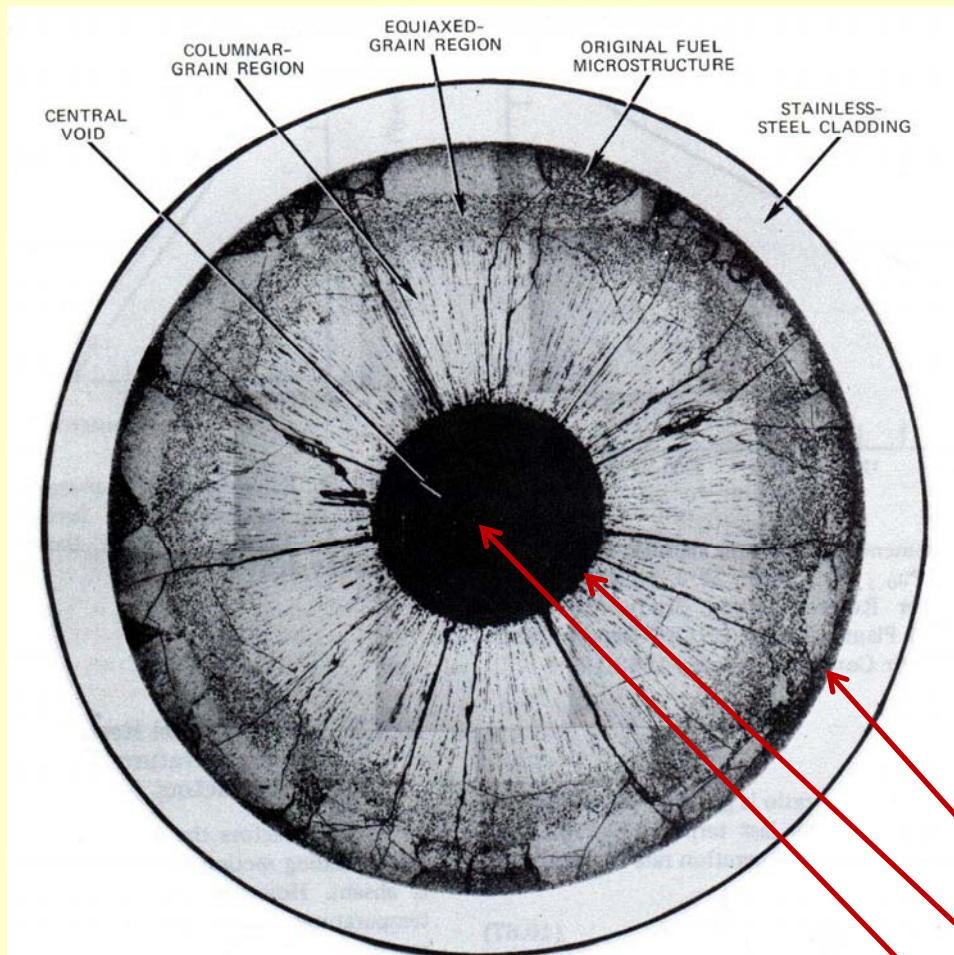# Example: Reactor pressure vessel embrittlement

C9900630-16

- fracture toughness of 800 ton RPV severely degraded by radiation-induced defect structure on a size scale of 2 to 5 nm
- DBTT shifts up to 200°C have been observed
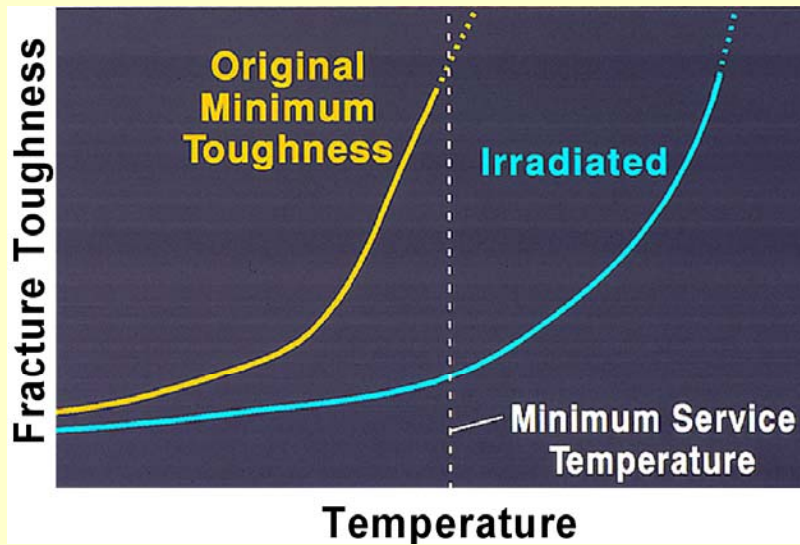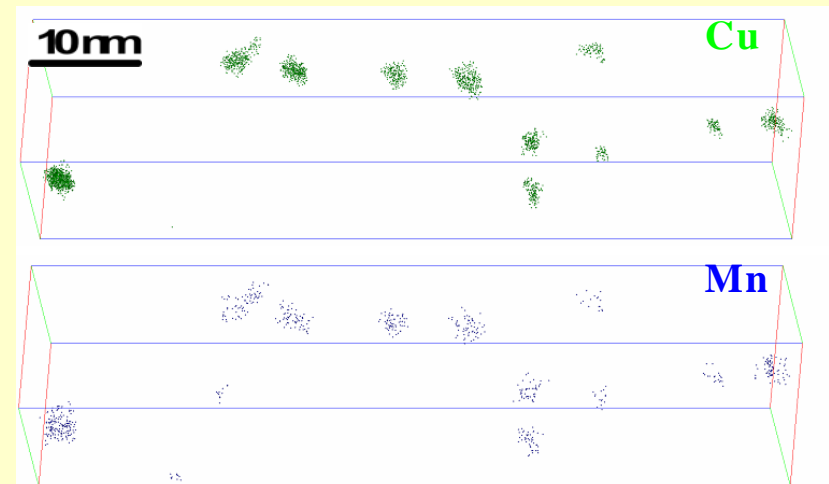
- Cu, (Mn, Ni, ...) –enriched solute clusters, neutron-irradiated RPV steel, APFIM data, M.K. Miller, ORNL

ornl

Example: Oxide fuel, UO$_2$

CENTRAL VOID

COLUMNAR-GRAIN REGION

EQUIAXED-GRAIN REGION

ORIGINAL FUEL MICROSTRUCTURE

STAINLESS-STEEL CLADDING

~1000°C

~2200°C

~2600°C

fuel pin radius ~3-4 mm

From Olander (1976, Fig. 10.22) Cross section of mixed-oxide fuel rod irradiated to 2.7% burnup.

- a combination of thermal and radiation-induced phenomena lead to massive restructuring at high linear powers (FBR fuel)

- UO$_2$ fission, "burn-up," leads to changes in fuel chemistry and stoichiometry

- radiation-enhanced diffusion, large temperature gradients (>10^3 °C/cm), and composition changes promote phase separation and density changes

- effects on physical properties such as thermal conductivity

ornl

Components of Primary Radiation Damage Source Term

- incident particles of different types and energies produce different types of primary damage
  - neutrons, heavy charged particles, electrons, photons
- produce differences in secondary damage accumulation
- need to know both energy spectrum and absolute flux level
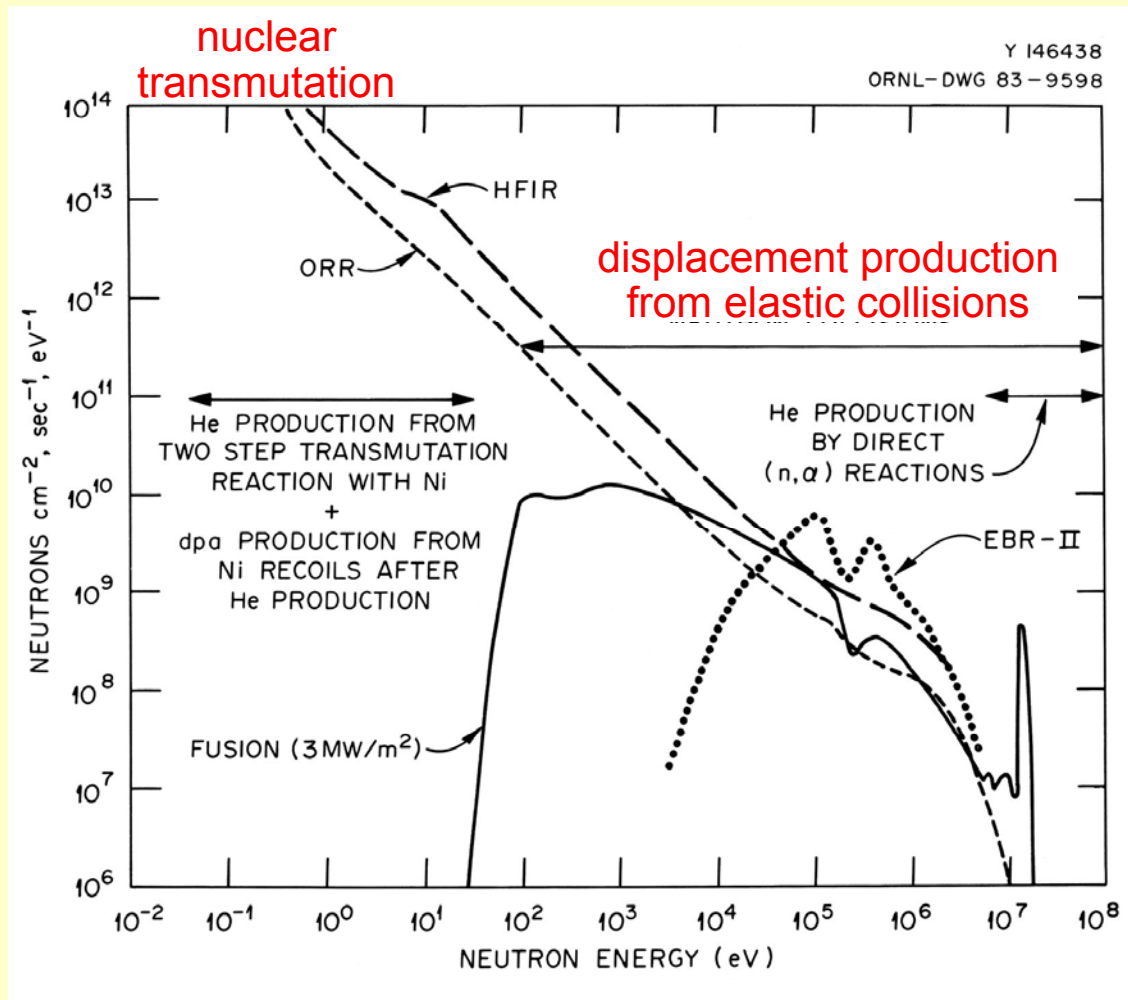
Primary Radiation Damage, con't.

I. Due to fission or fusion reactions

- "fission fragments", heavy charged particles recoiling from fission event
    - peaks around atomic masses 90 and 140
    - energy ~ 80-100 MeV
    - limited range, primarily impacts fuel
- high energy neutrons (flux >0.1 or >1.0 MeV traditionally used as correlation parameters by nuclear industry)
    - fission spectrum up to ~20 MeV, peak at ~0.65 MeV, ϕ(peak)/ϕ(10 MeV)~350
    - DT fusion at 14.1 MeV
    - displacement cross section minimum at ~1 keV (elastic scattering limit) for iron
- thermal neutrons
    - typically E<0.5 eV, kT_{room} = 0.025eV)
    - produce low energy recoils from (n,γ) capture reactions; a few 100s eV in steels

Primary Radiation Damage, con't.

- high energy (up to a few MeV) electrons
  - primarily produced by Compton scattering of fission gamma rays, some from (n,γ) reactions
  - generate low energy recoils (similar to thermal neutrons) by elastic scattering
  - displacements from either thermal neutrons or electrons can be significant in certain cases, e.g. HFIR RPV (e-), heavy-water (HFBR, Halden) or graphite moderated (MAGNOX) cores >

- nuclear transmutation products
  - gases: primarily hydrogen and helium from (n,p) and (n,α) reactions
  - solid: (n,p), (n,α), $(n,2n)$, (n,γ) with subsequent b decay
  - both thermal and high energy neutron reactions contribute
  - generally not too significant, appm to atom-% levels, but e.g. silicon production in aluminum where ϕ_{th}=2.5x10^{26} n/m^2 (~6 months in HFIR) converts 1% of Al to Si

Primary Radiation Damage, con't.

II. Due to accelerator based sources

- light and heavy ions
  - a few 100 keV to 5 MeV typical (up to ~40 MeV in cyclotrons)
- electrons, typically 1-5 MeV
  - used for illumination and damage production in HVEM *in situ* studies
- both ions and electrons have been heavily used in radiation damage "simulation" studies, combined ion-beam/TEM facilities
- modern spallation sources with proton energies ~1 GeV
  - substantial damage from primary proton beam
  - produce neutrons with energies up to nearly the beam energy
  - the periodic table of transmutation products, primary light elements with high levels of H and He
  - radiation effects research needed to predict performance of target materials, may be useful for some fusion materials investigation
  - significant need/opportunity for dosimetry experiments and calculations

Comparison of representative neutron and corresponding PKA energy spectra
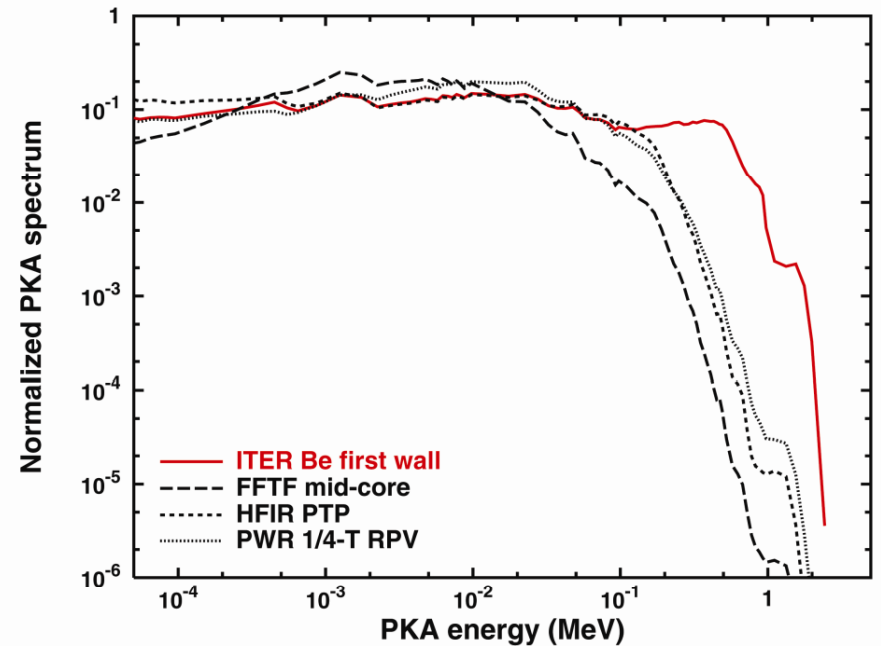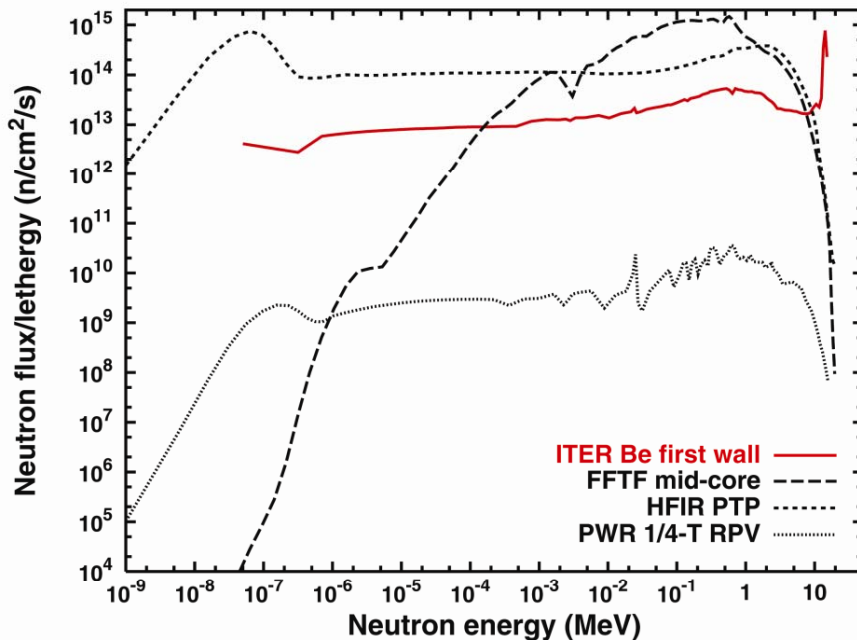
- differences in neutron flux level lead to different atomic displacement rates

- neutron energy spectrum differences lead to different PKA energy spectra
    - different coolants, water for HFIR and PWR vs. sodium for FFTF alter neutron energy spectrum, primarily influence lower energy
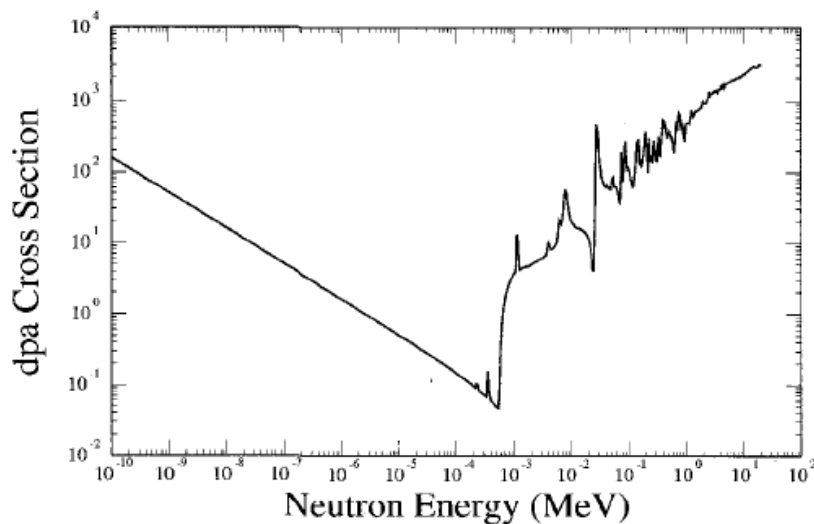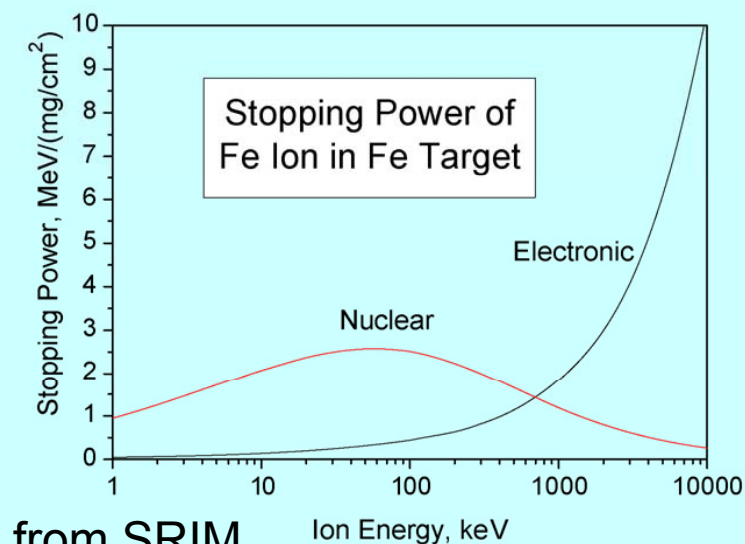   - high energy influenced by neutron source, c.f. all fission with ITER fusion

Energy dependence of damage deposition

FIG. 1 ENDF/B-VI-based Iron Displacement Cross Section

from SRIM

- energy dependence of dpa cross section integrates different phenomena

- electronic stopping generally ignored for neutron irradiation of metals
  - may be a factor for very high ion exposure, see literature on "swift heavy ions"
  - ratio of electronic to nuclear stopping power influences damage evolution in ceramics, e.g. fission tracks in UO_2

Molecular dynamics simulation of primary damage

- MD simulations provide opportunity to investigate displacement cascade evolution, e.g. effects of lattice, PKA energy, T, etc.

- Classical molecular dynamics, typical implementations:
  - many millions of atoms, solve Newton's equation of motion
  - constant pressure or volume, periodic boundary condition
  - system may or may not be thermostated to prevent PKA from heating system
  - no electronic losses or electron-phonon coupling, energy of cascade simulation

- to compare with standard NRT displacement model:**

  $\nu_{NRT} = 0.8\,T_{dam}/(2\,E_d)$, T_{dam} = kinetic energy lost in elastic collisions

  - $E_{MD} \sim T_{dam}$ (NRT) $< E_{PKA}$
  - e. g. for T_{dam} = 100 keV, E_{PKA} = 175.8 keV and ν_{NRT} = 1000

** **For a good summary, see D. R. Olander, "Fundamental Aspects of Nuclear Reactor Fuel Elements," 1976**

Ratio of damage energy (T_d) to PKA energy (E_{PKA}) as a function of PKA energy \
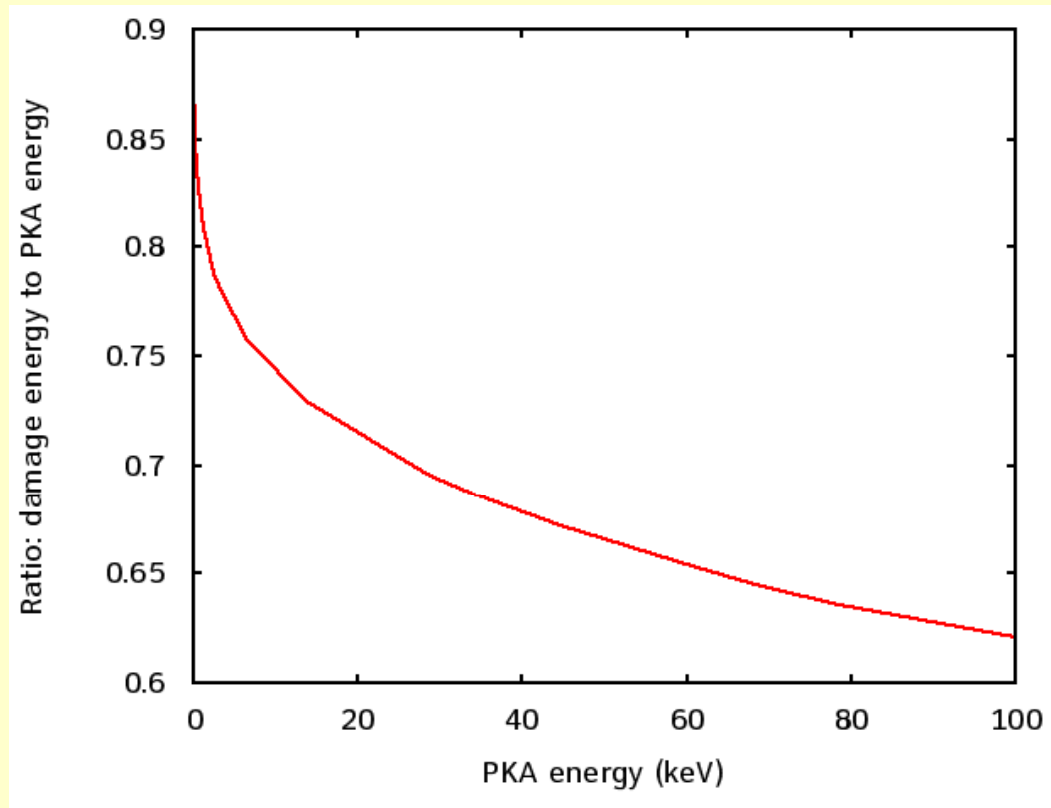
Note that even at low energies a significant fraction of the PKA energy goes into electronic excitation and ionization

Parameters for elastic collisions in iron based on NRT and LSS models

Neutron Energy (MeV)	Average PKA Energy (keV), E_{PKA}	Damage Energy (keV), T_{dam}	NRT Displacements	T_{dam}/E_{PKA}
0.003351	0.1158	0.100	1.0	0.8634
0.006818	0.2357	0.200	2.0	0.8487
0.01749	0.6046	0.500	5.0	0.8269
0.03578	1.237	1.000	10.	0.8085
0.07342	2.538	2.000	20.	0.7881
0.1911	6.605	5.000	50.	0.7570
0.3968	13.71	10.00	100.	0.7292
0.8321	28.76	20.00	200.	0.6954
2.277	78.69	50.00	500.	0.6354
5.085	175.8	100.0	1000.	0.5690
12.31	425.5	200.0	2000.	0.4700
14.10	487.3	220.4	2204.	0.4523

Note: 48 keV is average PKA energy for ITER First Wall

MD cascade database for iron

- an extensive cascade database has been developed that covers a broad range of cascade energy and temperature
  - up to 200 keV at 100, 600, and 100 keV at 900K
- this database includes a sufficient number of simulations at each condition to provide a good statistical measure of average cascade behavior
  - total number of point defects produced
  - in-cascade clustering fractions for both interstitials and vacancies
  - in-cascade cluster size distributions
  - Note: nature of cascade event leads to better statistics for defect production than for clustering
- common use of Finnis-Sinclair potential provides basis for comparison other investigations:
  - pre-existing damage (relevant to cascade overlap) using 10 keV cascades
  - free surfaces (relevant to in situ experiments) using 10 and 20 keV cascades
  - nanograined iron using 10 and 20 keV cascades

Fe Cascade Database at 100K (fewer at 600 and 900K)

Cascade Energy (keV)	Number of Simulations	Typical cell size (atoms)
0.1	40	3,456
0.2	32	6,750
0.5	20	16k/54k
1.0	12	54k
2.0	10	54k
5.0	9	128k
10.	15	125k/250k
20.	10	250k
30.	10	432k
40.	8	1.024M
50.	9	2.249M
100.	10 [20@600K, 18@900K]	5.030M
200.	9	up to 21.16M

Illustrate defects of interest from simulations
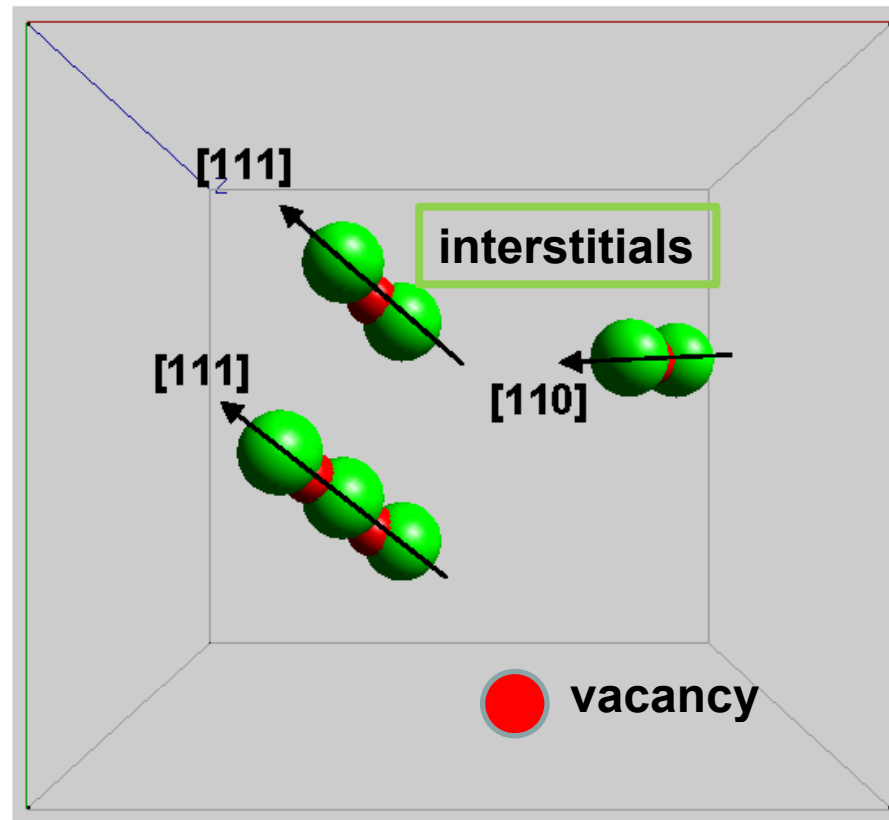
Figure 3. Typical configurations for interstitials created in displacement cascades: [110] and [111] dumbbells and [111] crowdion.

Time dependence of defect evolution in atomic displacement cascades
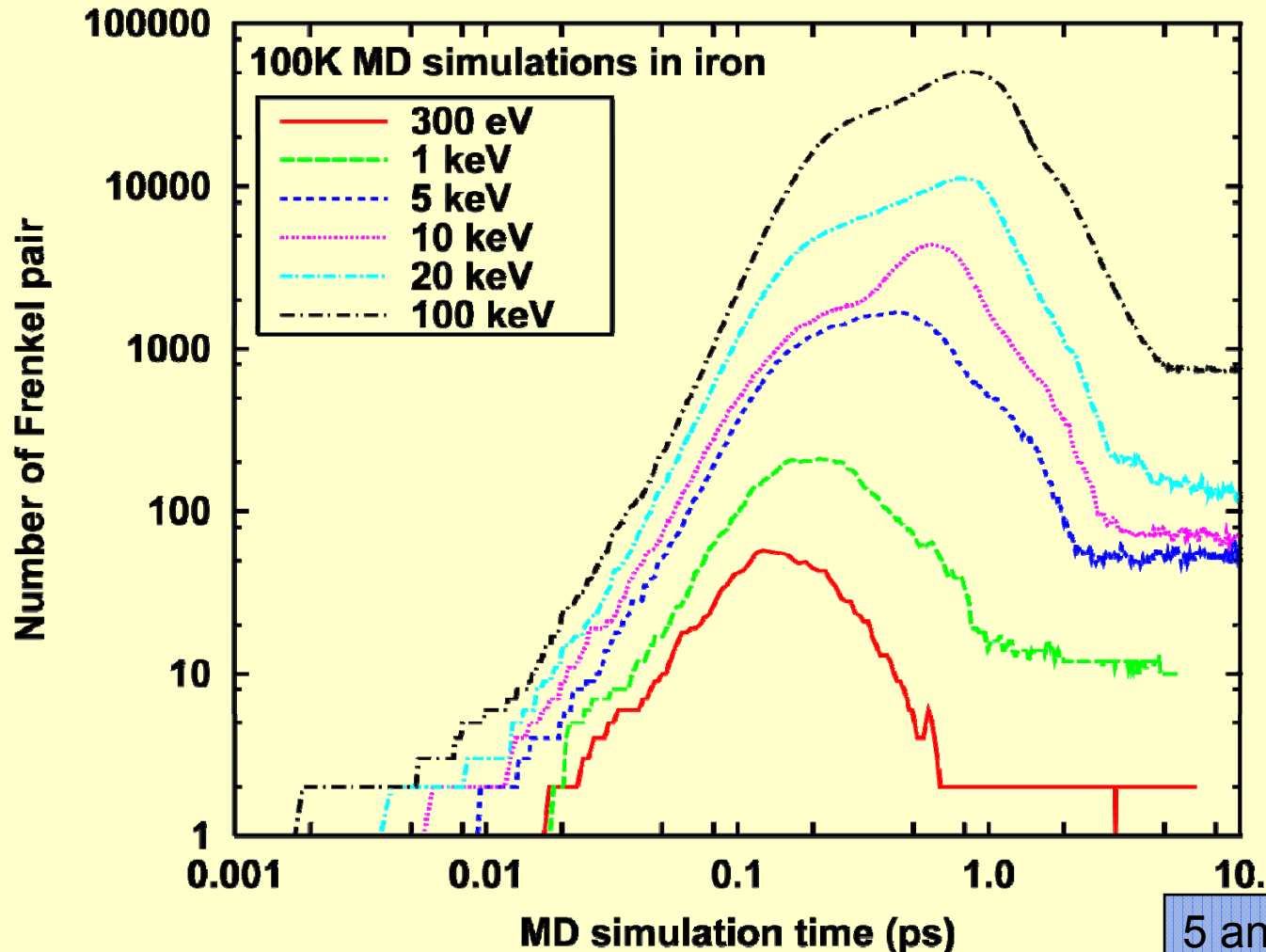
5 and 50 keV examples

Angular dependence of displacement threshold energy: effect of crystalline lattice on defect formation

classical MD

Fe

V
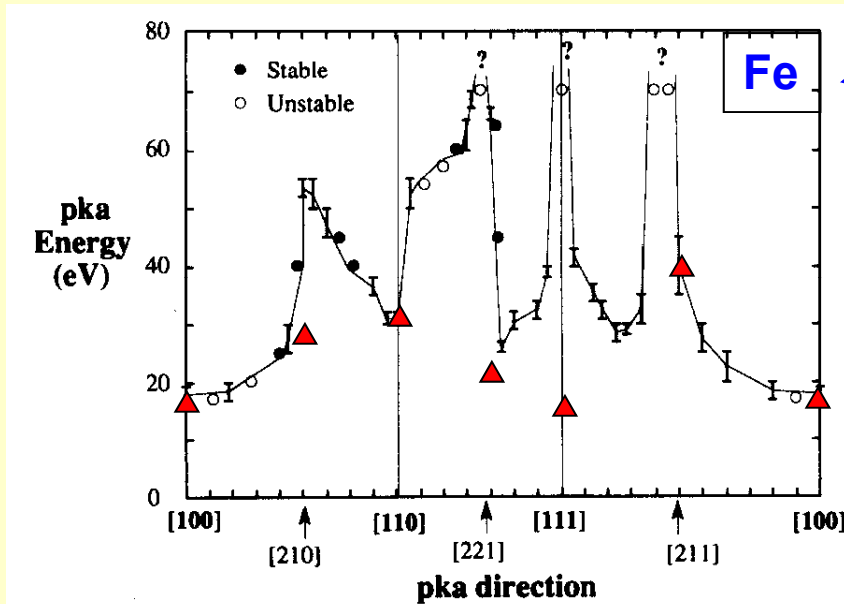
Fig. 4. Displacement threshold curve for α-Fe at 0 K. Data points for directions without error bars indicate the lowest/highest PKA energy that produced a stable/unstable Frenkel pair.

Bacon, et al., JNM 205, 1993

FIG. 2. Variation of the threshold displacement energy (TDE) with recoil orientation and temperature from the MD simulations (open symbols). Experimental measurements for Fe (Ref. 22) and Mo (Ref. 23) are also shown for comparison. The dashed line is a guide connecting the average of the MD results.

Zepeda-Ruiz, PRB 67, 2003

▲ *ab initio MD*, P. Olsson, C. Domain, EDF R&D

ornl

In contrast to linear damage energy dependence of NRT model, three well defined energy regimes appear

- at lowest energies true "cascade-like" behavior does not occur
- above ~10 keV, subcascade formation dominates
- nearly linear energy-dependence is observed at higher energies, consistent with simple reasoning of K-P or NRT models
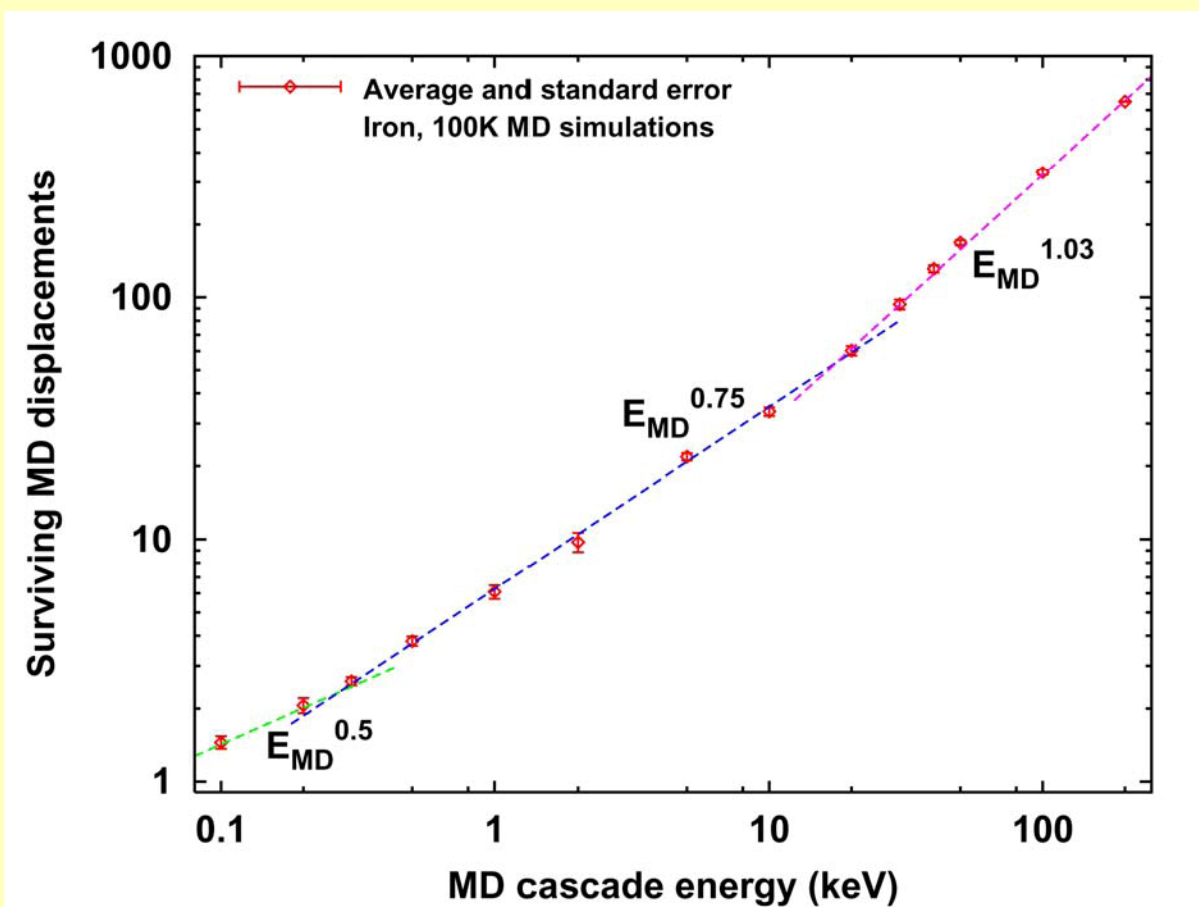
If normalized to NRT displacements, MD results show reduced defect survival as cascade energy increases
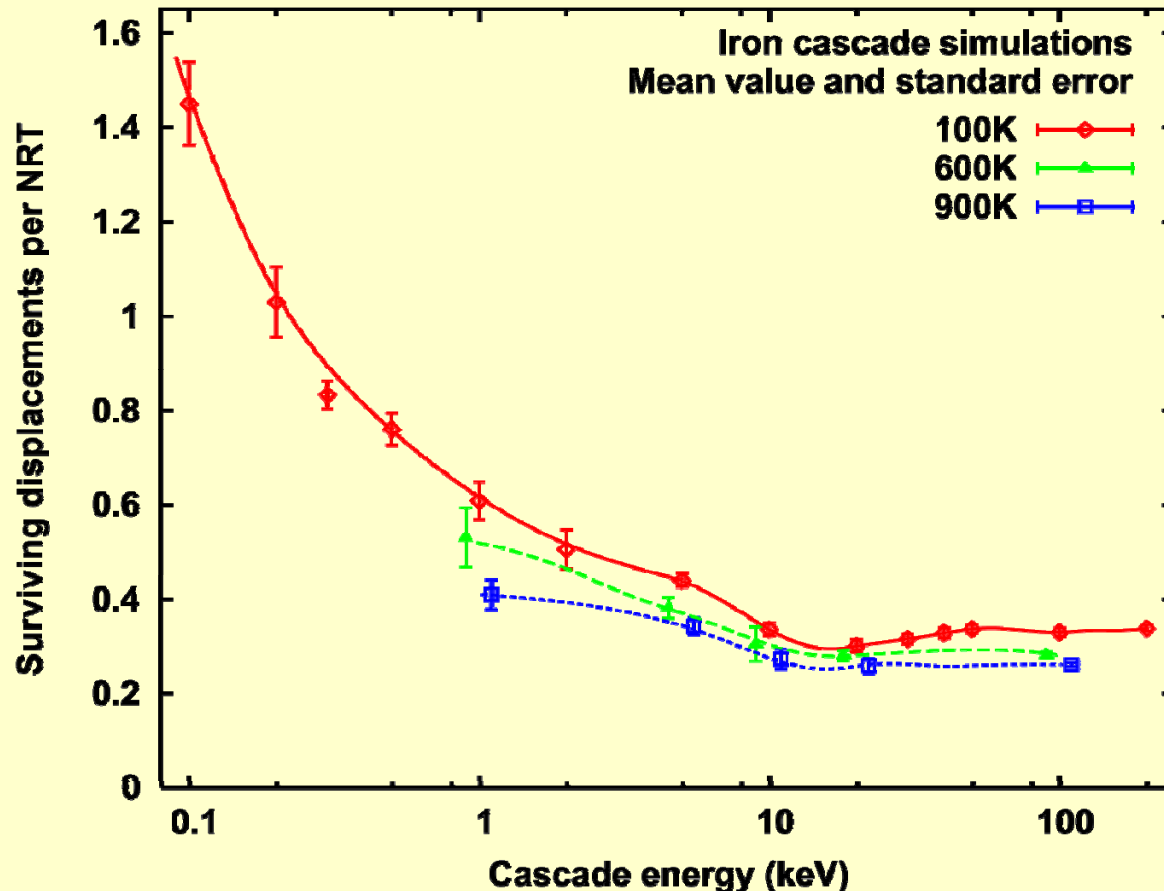
- some of curve structure is significant, related to cascade morphology and subcascade formation
- note small standard errors, measure of mean behavior
- effect of temperature, 100 to 900K, is systematic but not strong

Many of surviving defects are in clusters formed during the cascade event

vacancy
interstitial

20 keV, 600K

33 interstitials, glissile
1D configuration
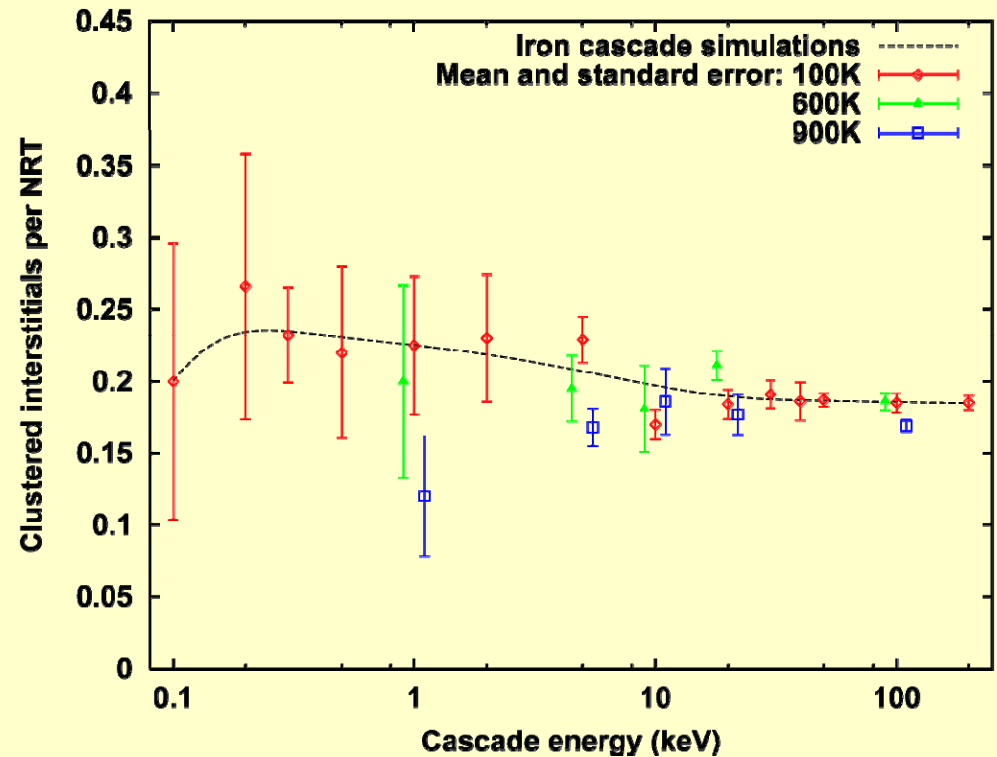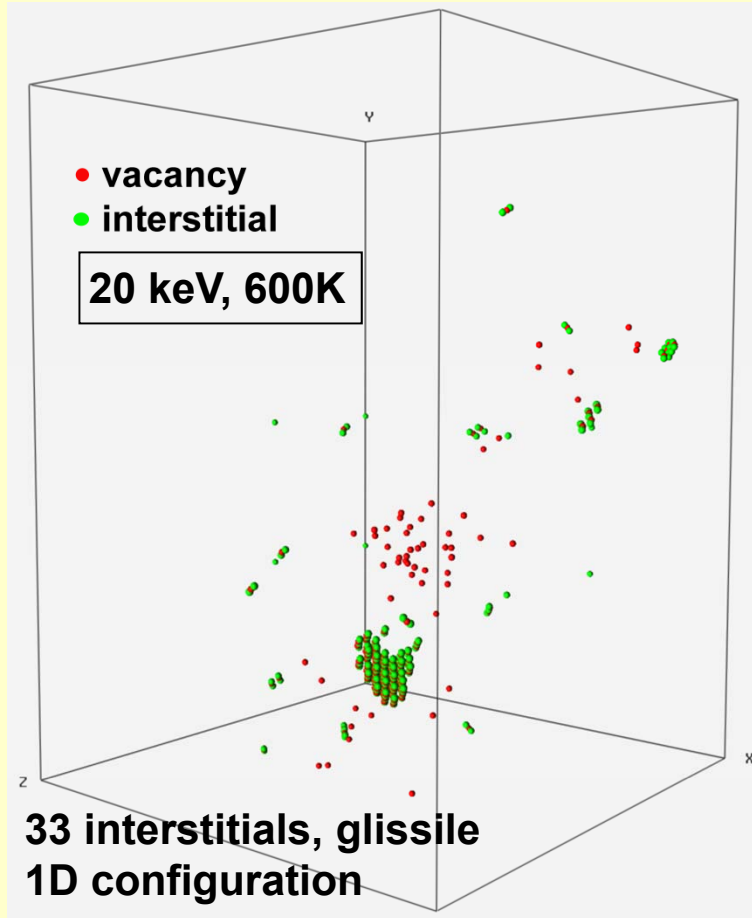
Note: poorer statistics, larger standard errors, than for total defect survival

- significant in nucleation of extended defects
- not accounted for by dpa (or ϕ >x MeV)

20 keV examples

Illustration of subcascade structure at peak damage condition for cascades at 100K
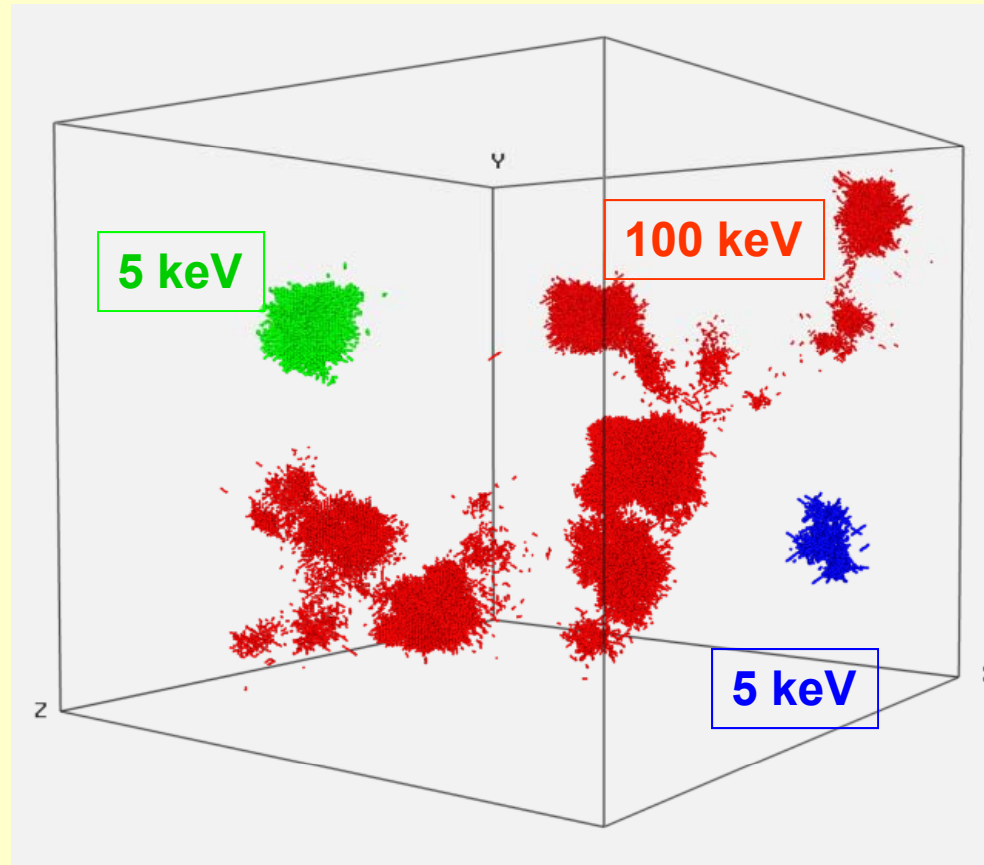
- high energy cascades look like multiple lower energy events, leads to asymptotic behavior with energy
- low energy events between subcascades have higher efficiency

Influence of energy and temperature on SIA clustering
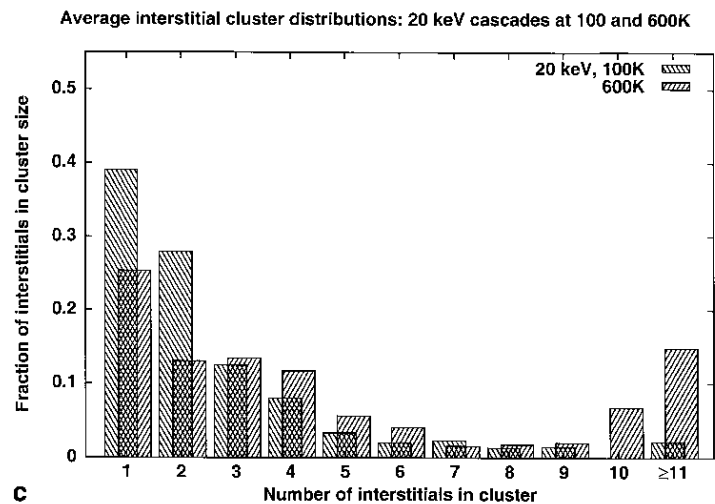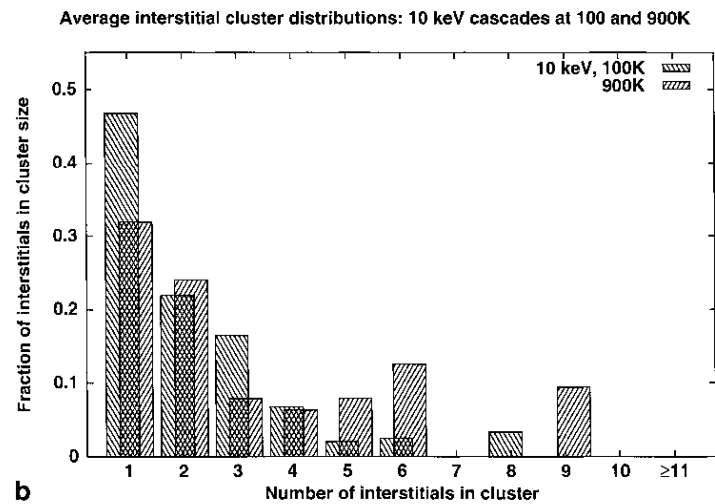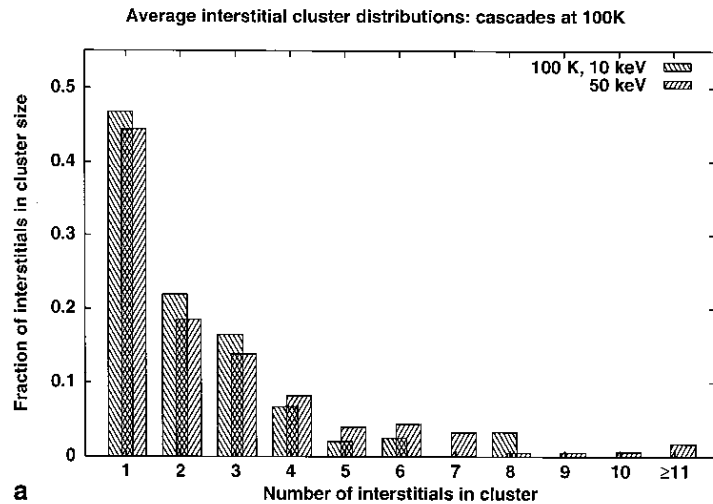
Fig. 4. Fractional size distributions of interstitial clusters formed directly within the cascade, comparison of: (a) 10 and 50 keV cascades at 100 K; (b) 10 keV cascades at 100 and 900 K; (c) 20 keV cascades at 100 and 600 K.

Stoller, JNM 276, 2000

Vacancy clustering in iron

- MD simulations reveal little vacancy clustering in the nearest-neighbor sense - but, vacancies are spatially correlated
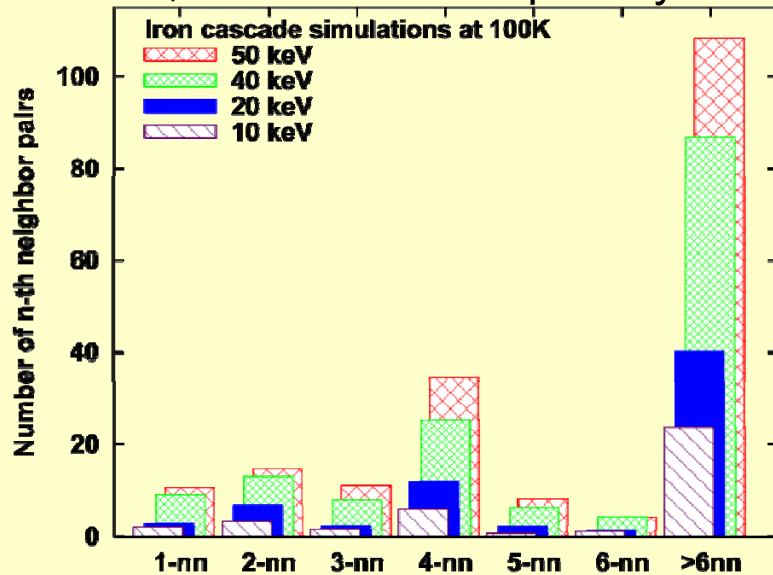
Typical uncollapsed vacancy cluster, 50 keV cascade at 100 K

arrows indicate 4nn
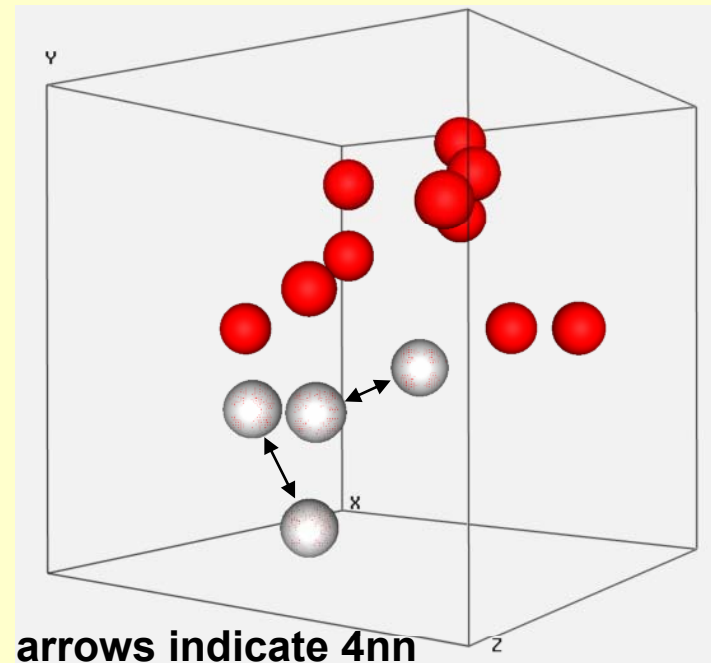
- kMC aging of residual defects indicate that such loose or nascent clusters do tend to collapse into void-like configurations
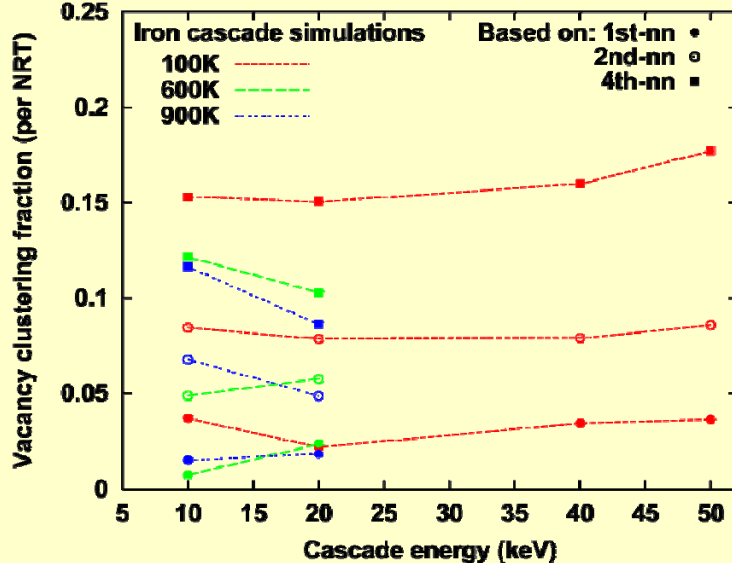
# Influence of energy and temperature on vacancy clustering
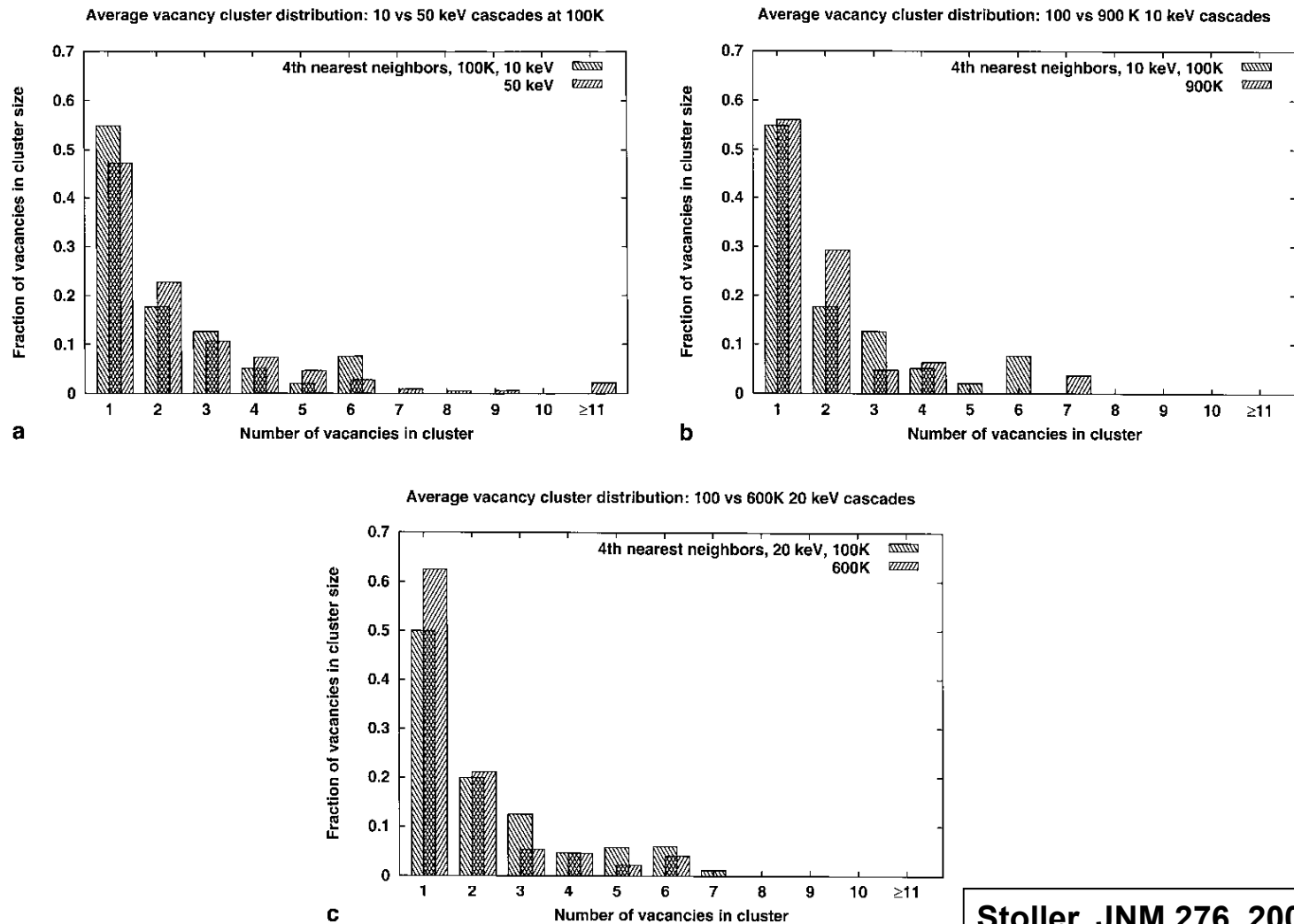
Fig. 9. Fractional size distributions of loosely coupled vacancy clusters (all within 4-nn) formed directly within the cascade, comparison of: (a) 10 and 50 keV cascades at 100 K; (b) 10 keV cascades at 100 and 900 K; (c) 20 keV cascades at 100 and 600 K.

Stoller, JNM 276, 2000

Spectrum-averaged defect production

How do we compare or correlate data from different irradiation conditions?

- recall neutron and PKA energy spectra comparison above
- NRT dpa provide one basis for comparison alternate is to fit energy-dependent MD defect formation curves
- defect survival varies only weakly between different reactor environments

Neutron-energy-spectrum average

Neutron-energy-spectrum average

Neutron-energy-spectrum average
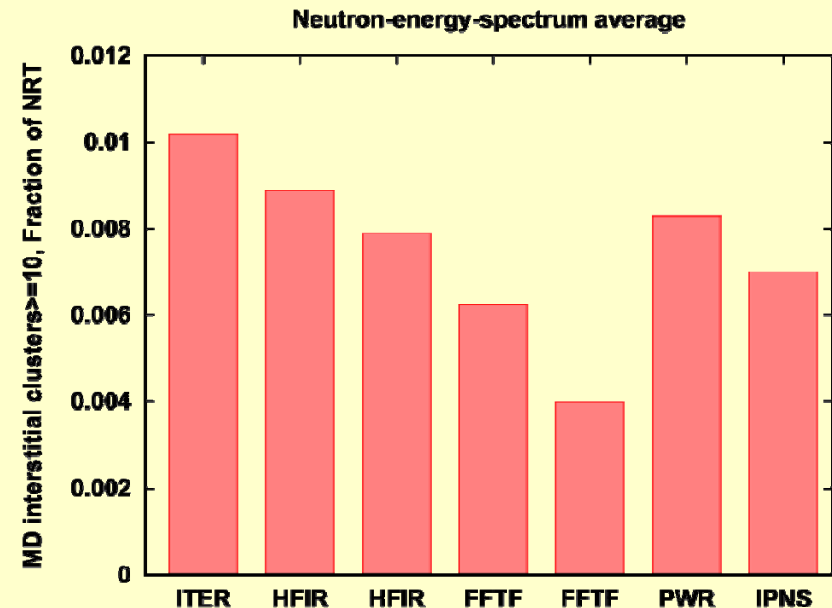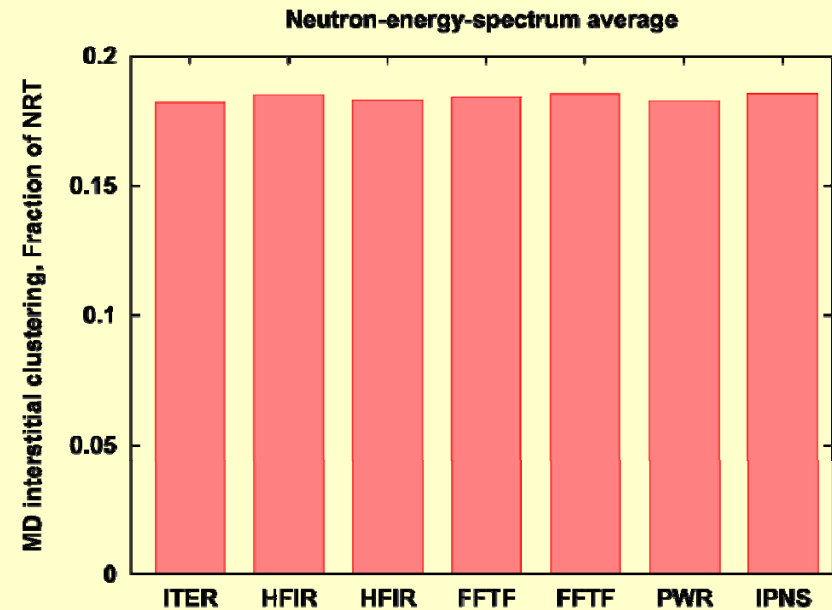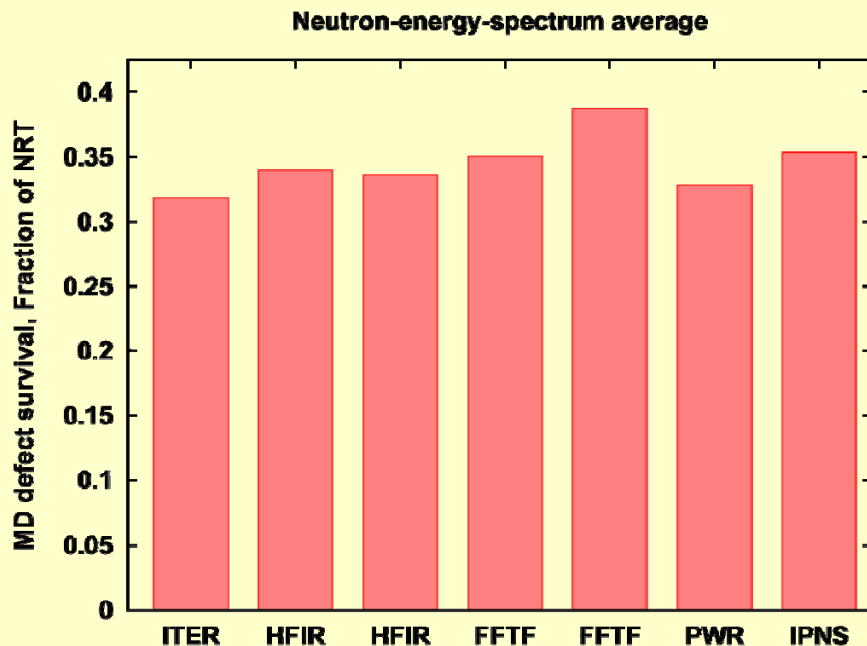
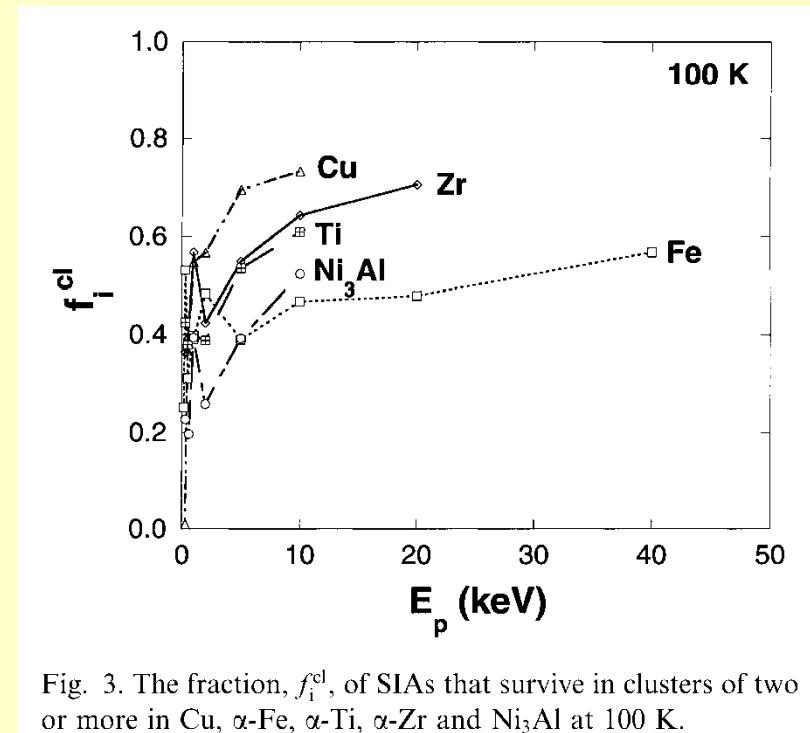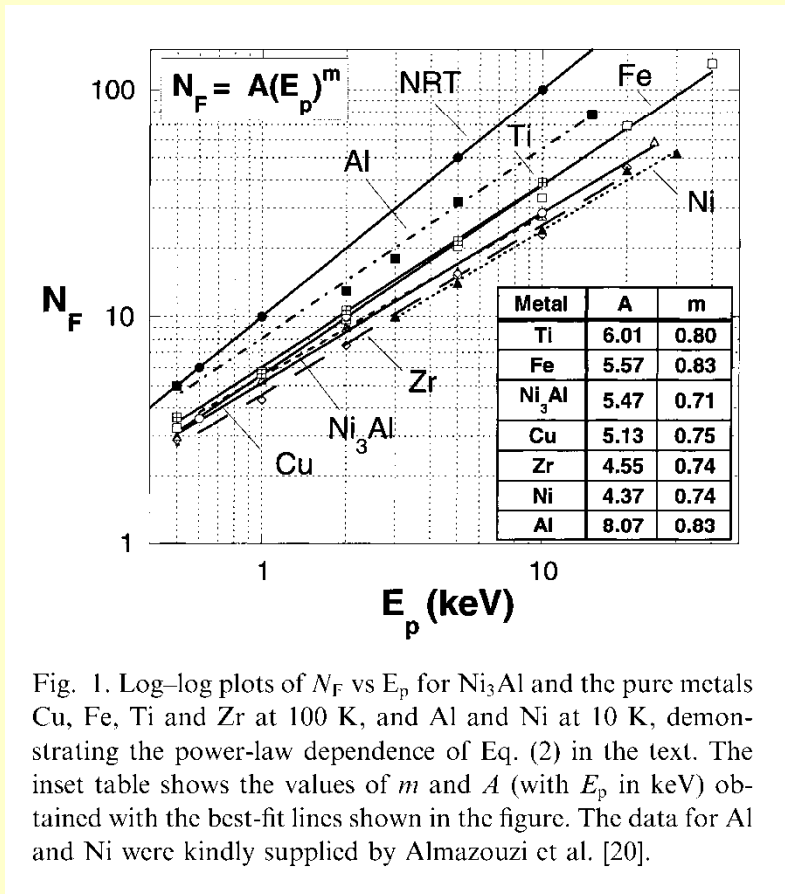# Comparison of 10 keV cascades in iron and copper based on molecular dynamics simulations
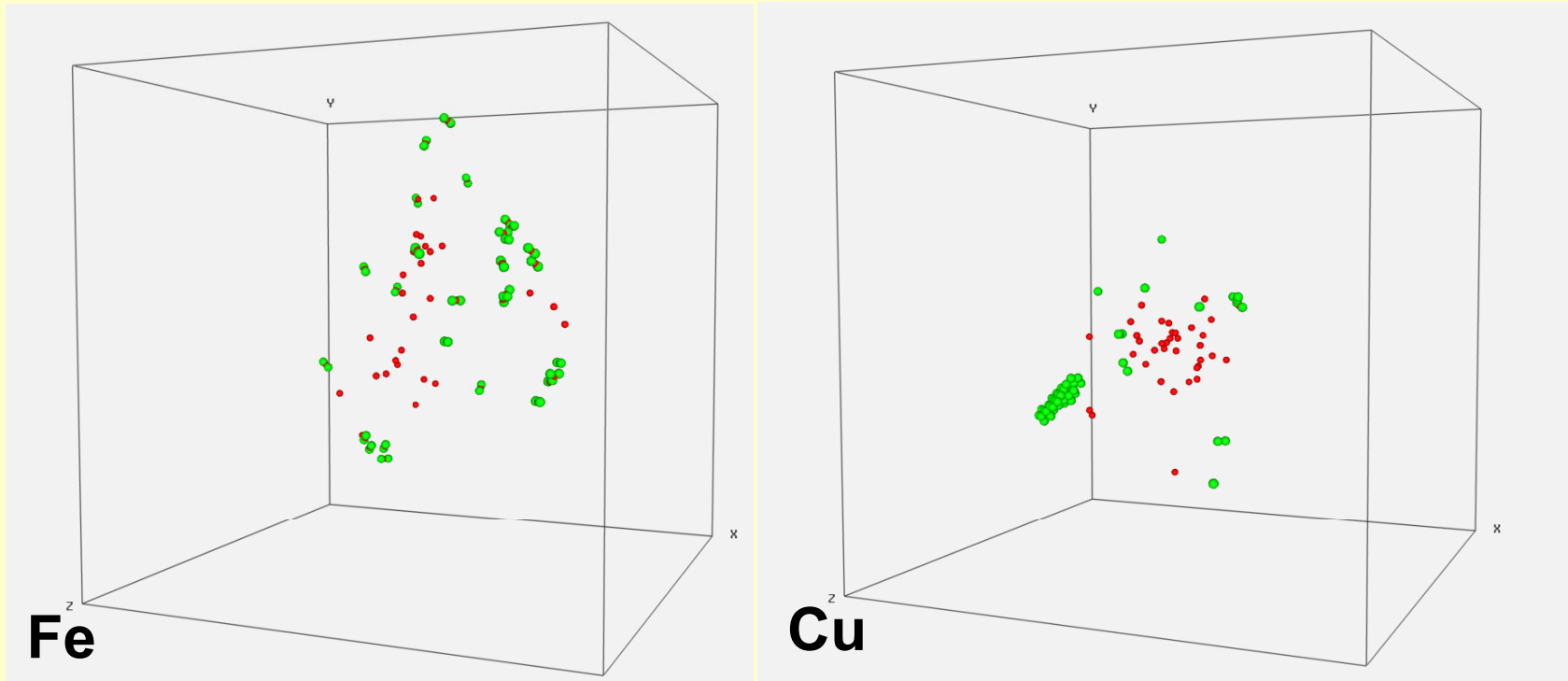
- Similar embedded atom type interatomic potentials, edge length of simulation cells is $50a_o$.
- Note higher level of in-cascade clustering in more-compact copper cascade.
- Defect survival (relative to NRT) is lower in copper than in iron.

Comparison of 20 keV cascades in iron and copper based on molecular dynamics simulations

Fe

Cu

20 keV, 100K Iron

20 keV, 100K Copper
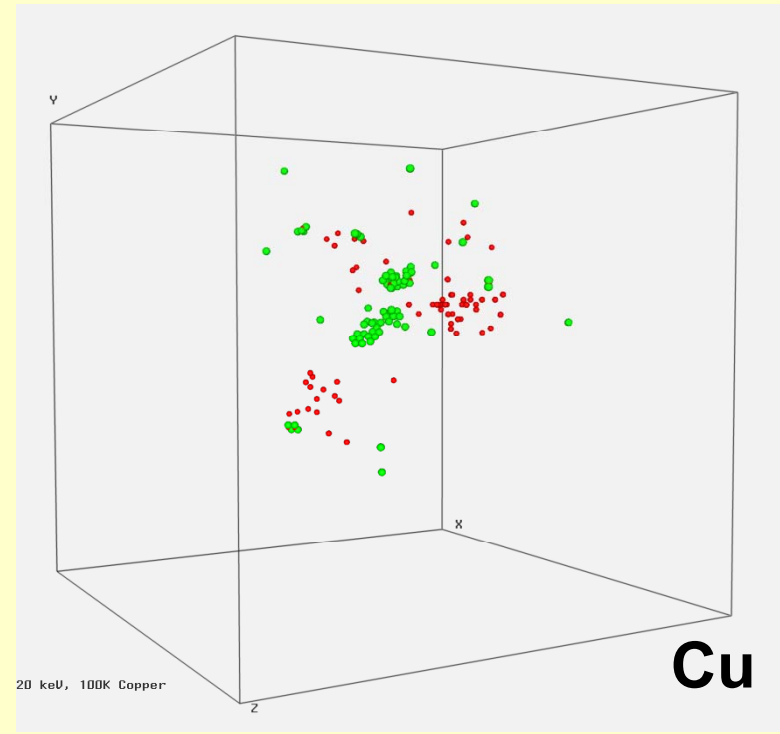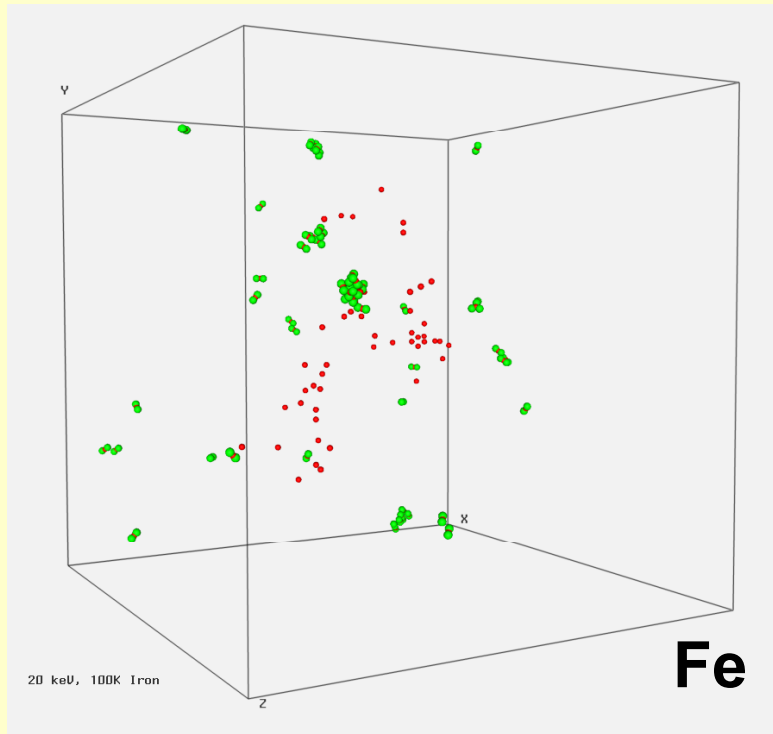
- Similar embedded atom type interatomic potentials, edge length of simulation cells are $50a_o$.
- Note higher level of in-cascade clustering in more-compact copper cascade.
- Defect survival (relative to NRT) is lower in copper than in iron.

Comparison of MD defect formation in a range of bcc, fcc, and hcp metals

Fig. 1. Log–log plots of N_F vs E_p for Ni$_3$Al and the pure metals Cu, Fe, Ti and Zr at 100 K, and Al and Ni at 10 K, demonstrating the power-law dependence of Eq. (2) in the text. The inset table shows the values of m and A (with E_p in keV) obtained with the best-fit lines shown in the figure. The data for Al and Ni were kindly supplied by Almazouzi et al. [20].

Fig. 3. The fraction, f_i^{cl}, of SIAs that survive in clusters of two or more in Cu, α-Fe, α-Ti, α-Zr and Ni$_3$Al at 100 K.

Bacon, et al, JNM 276, 2000

- different values, but similar power-law depending in defect survival
- energy dependence of SIA clustering similar, varies by a factor <2

Similar defect production results obtained in UO$_2$
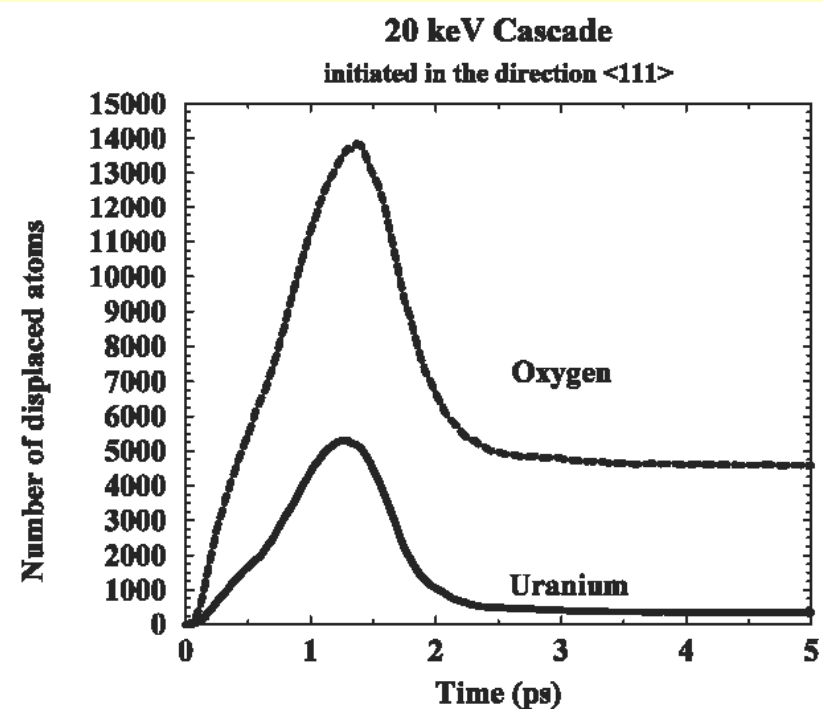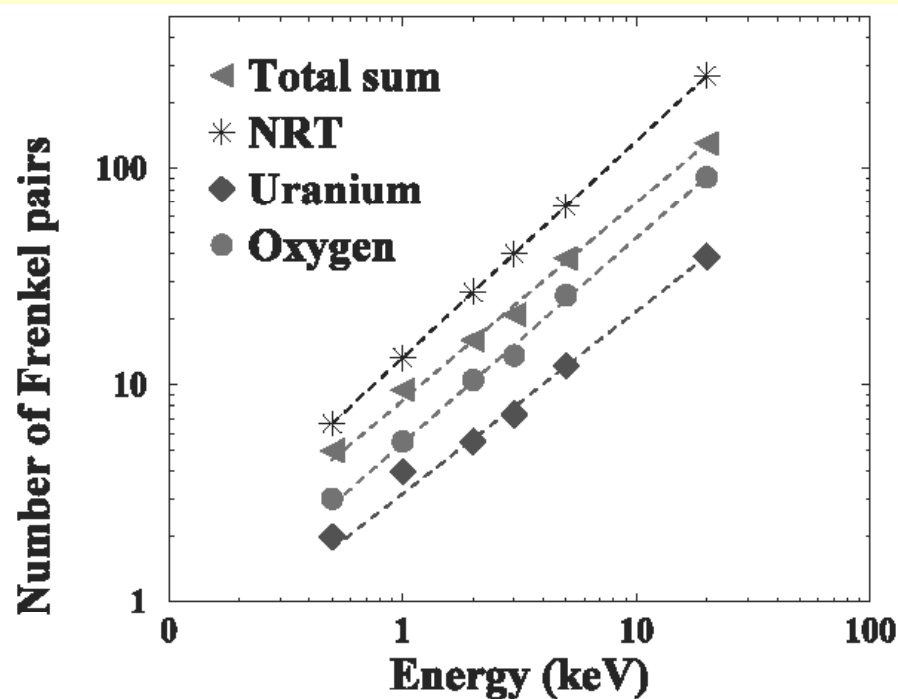
- defect production values different on U and O sublattices
- greater uncertainty concerning validity of empirical interatomic potential
- neglect of electronic effects may be more significant

(results from Van Brutzel, et al., Phil. Mag., 2003)

In-cascade clustering in UO$_2$ also similar to cascade production in metals
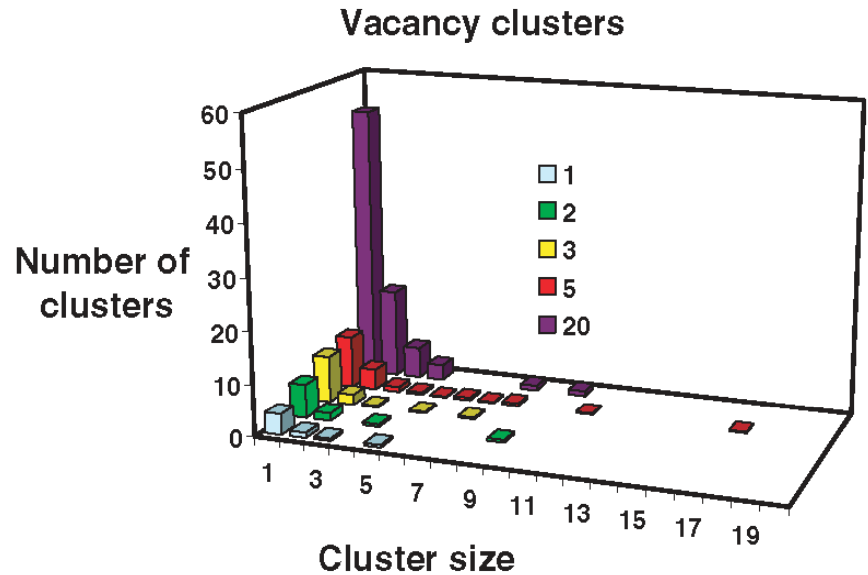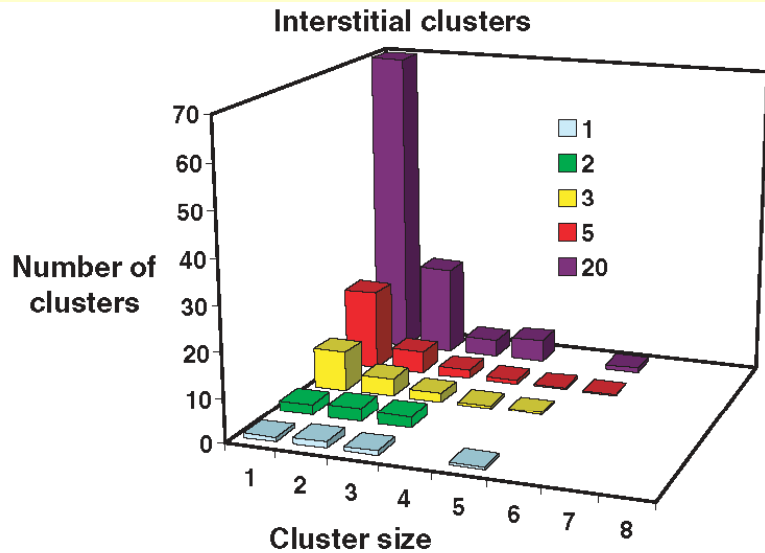
15.   Number of interstitial cluster versus the initial energy of the PKA. Figure 14.   Number of vacancy cluster versus the initial energy of the PKA.
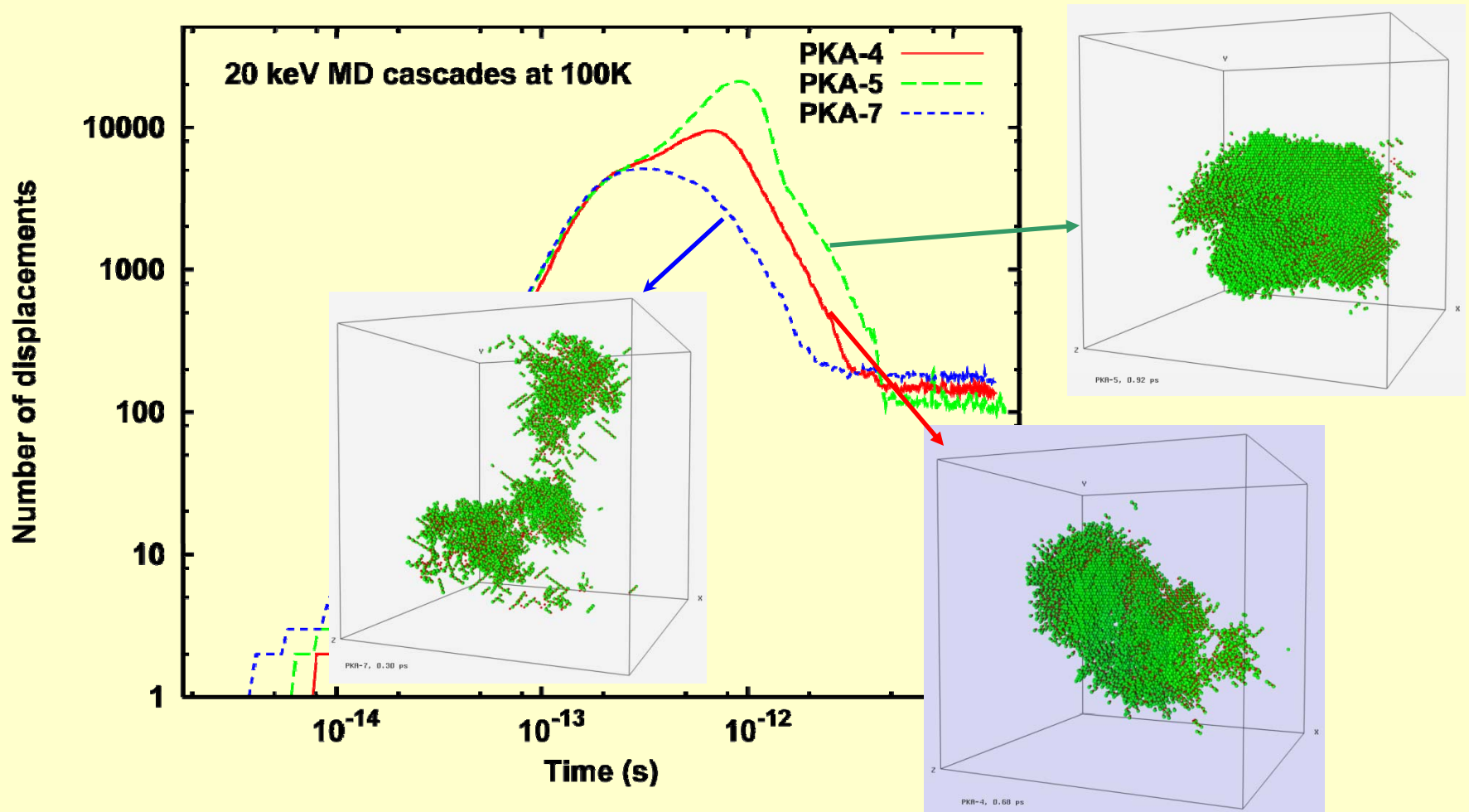
(results from VanBrutzel, et al., Phil. Mag., 2003)

ornl

Influence of cascade structure on time signature

20 keV MD cascades at 100K

PKA-4
PKA-5
PKA-7

Number of displacements
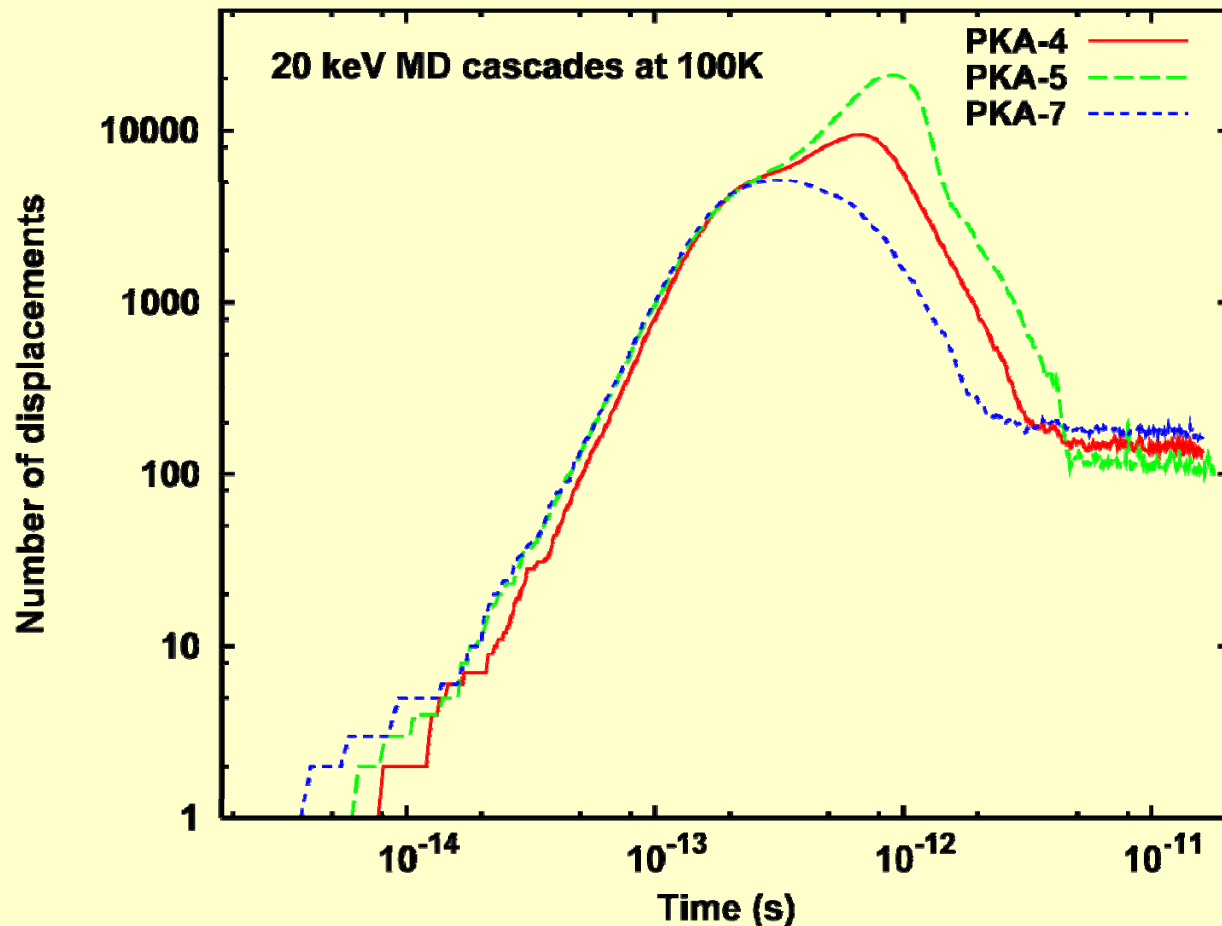
Time (s)

- systematic differences in the time dependence of defect formation are observed around the time of peak damage

Influence of cascade structure on time signature

20 keV MD cascades at 100K

PKA-4
PKA-5
PKA-7

Number of displacements

Time (s)

PKA-5, 0.92 ps

PKA-7, 0.30 ps

PKA-4, 0.60 ps

- subcascade formation reduces influence of pressure wave that creates many small-range, transient displacements
- note that stable defect formation is reduced for structures with higher peak values

pressure wave movie

Formation of point defect clusters

Calder, et al. (Phil. Mag. 90, 2010) have carried out detailed analysis of high-energy cascades. By tracking individual atoms, and local temperature and atom density, they show:

- the formation of large SIA clusters in Fe is related to the formation of hypersonic recoils (>10 speed of sound) near the sonic front of the primary cascade

- site of the SIA cluster is determined within ~0.1 ps
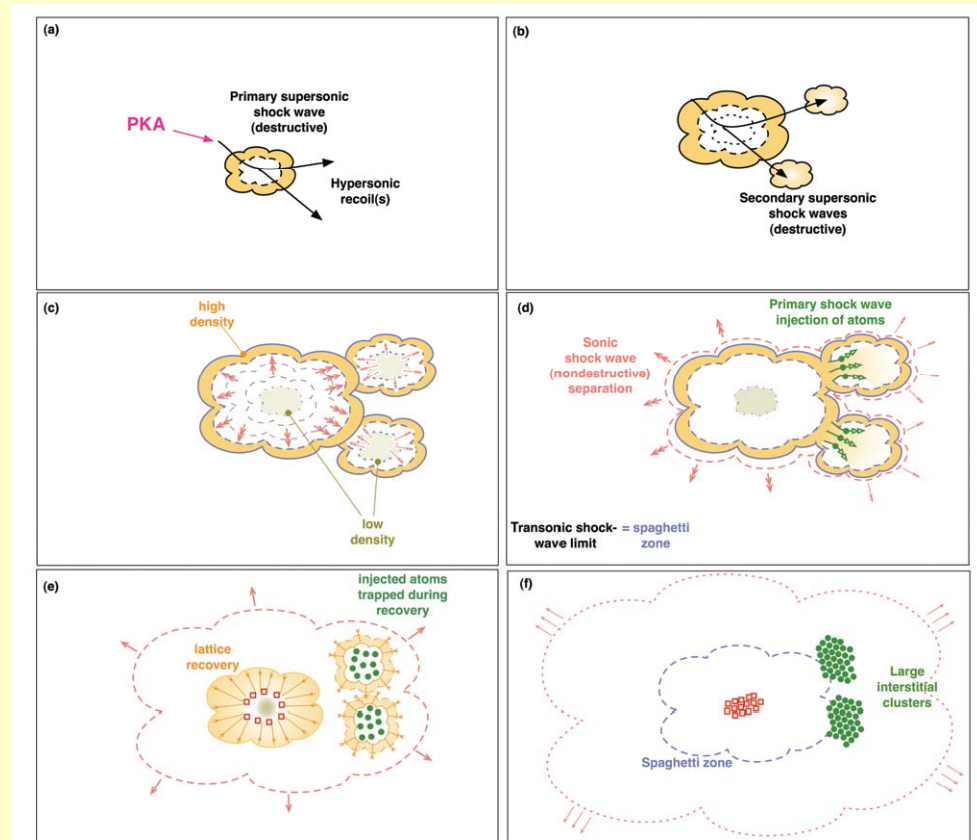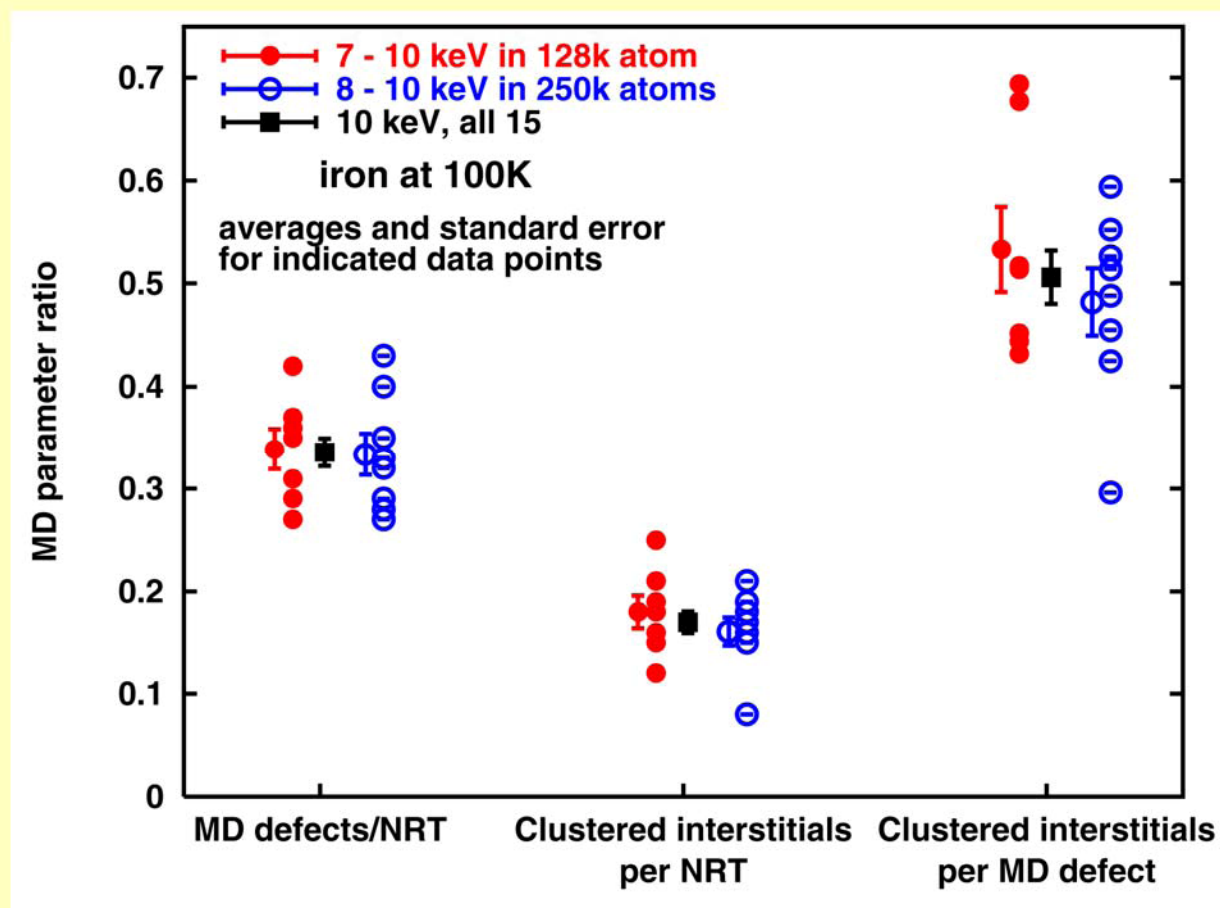
- vacancy cluster collapse is a result of prior SIA clustering

Figure 11. (Colour online). Schematic representation of cascade development over time and interstitial cluster formation.

Statistical variations in database: 10 keV

- larger energies require fewer simulations to obtain mean behavior
- NRT normalization produces smaller standard error for interstitial clustering than does normalization to MD defect survival

Statistical variations: 100 keV cascades at 600 K
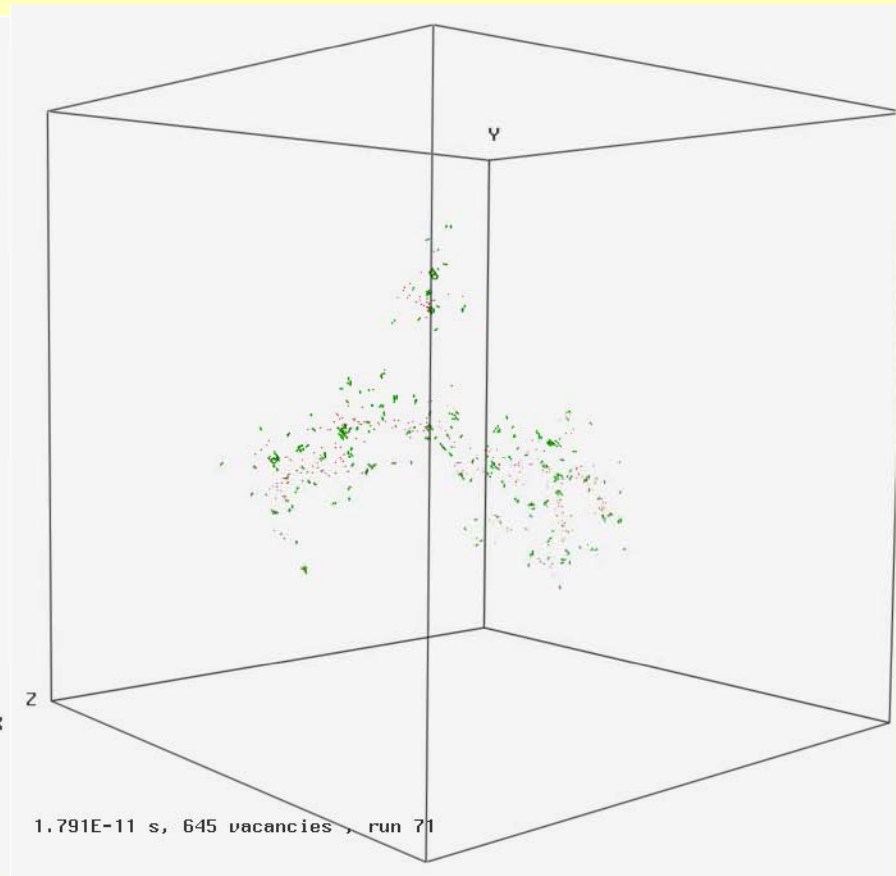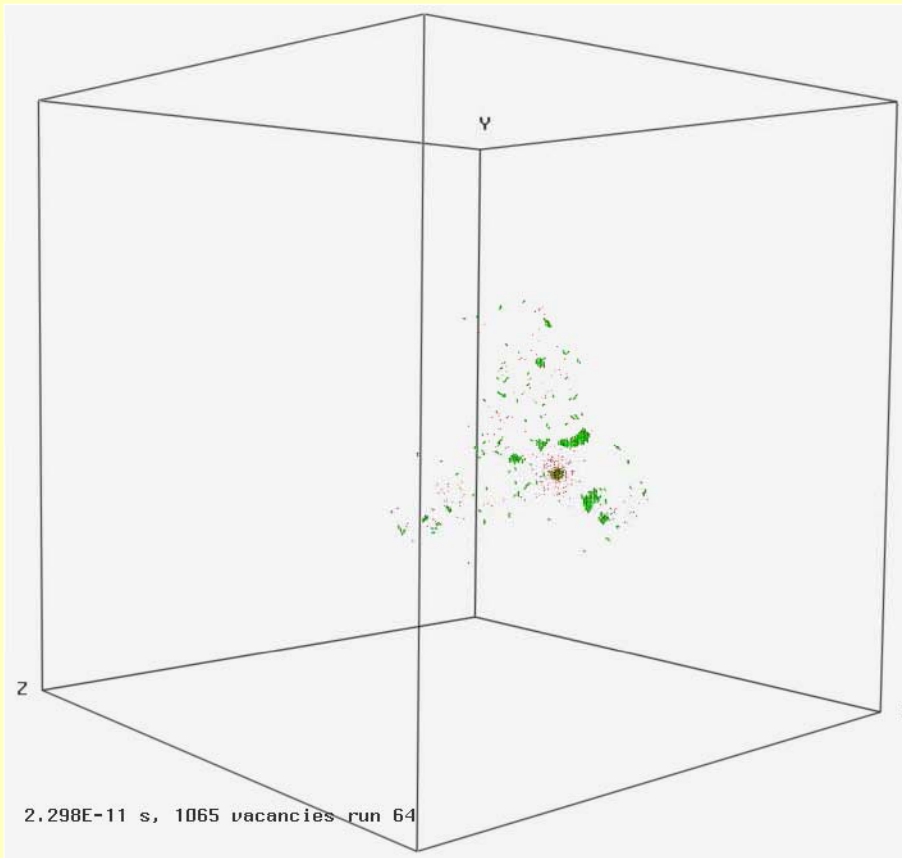
- **compact cascade: ~340,000 'defects' at peak, 326 FP survive, large clusters**

- **diffuse cascade (channeling): ~49,000 'defects' at peak, 301 FP survive**

Major difference between high-energy cascades: interstitial cluster size distribution
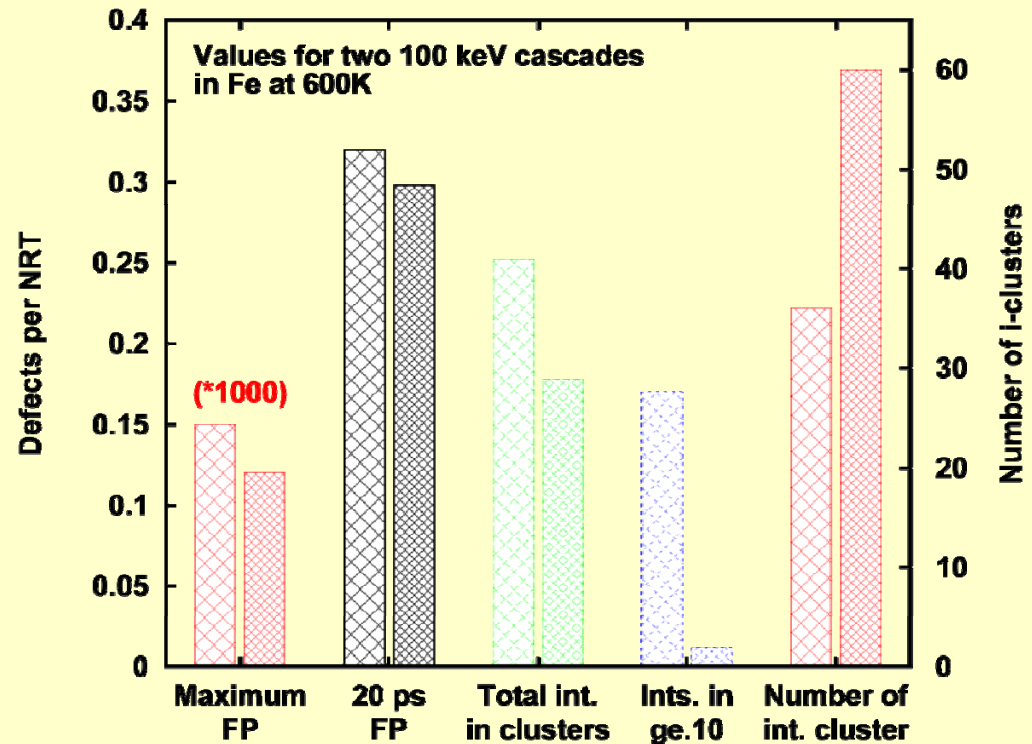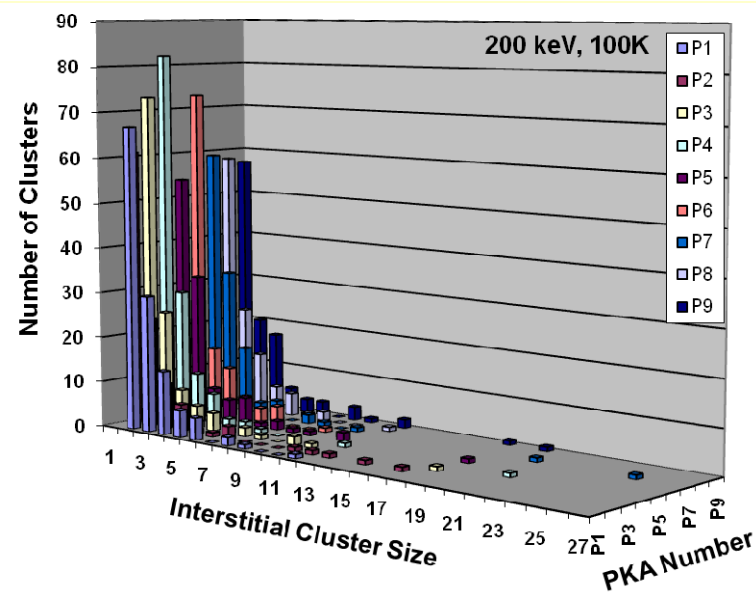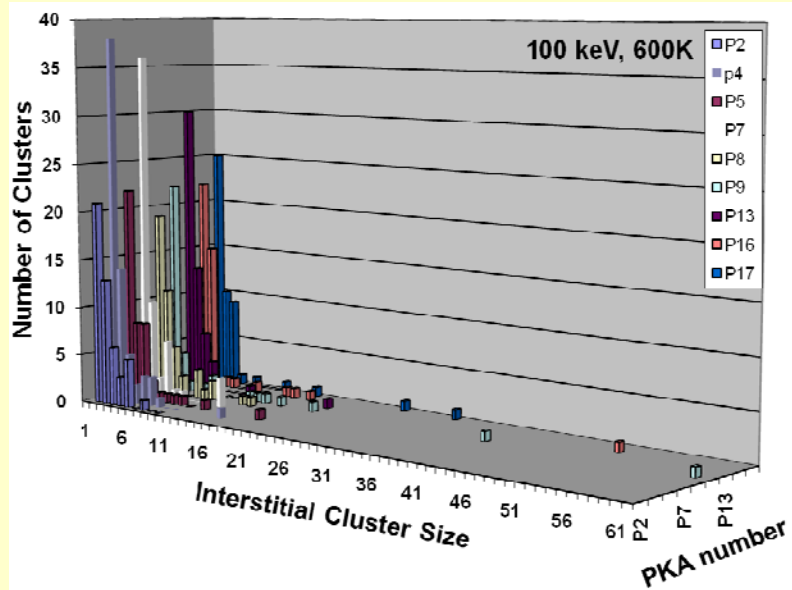
Influence of Pre-Existing Cascade Damage

- 10 keV simulations at 100K

- perfect crystal database consists of 7 simulations in 128k atom cells and 8 simulations in 250k atom cells

- three sets of simulations were carried out to investigate different types of pre-existing cascade damage

  - as-quenched cascade debris from 10 keV cascade in perfect crystal, total of 30 vacancies and interstitials, includes 1 di-interstitial and 1 7-interstitial cluster

  - similar case above, but some of the vacancies rearranged into a 6-vacancy void and a 9-vacancy loop
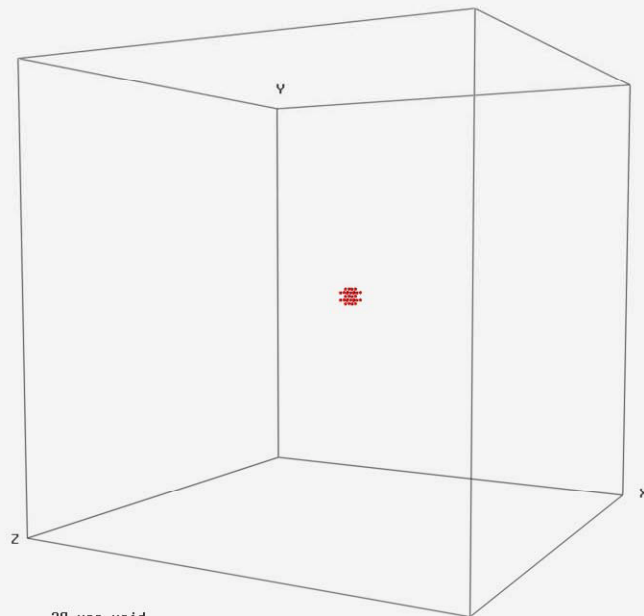
  - a single 30-vacancy void

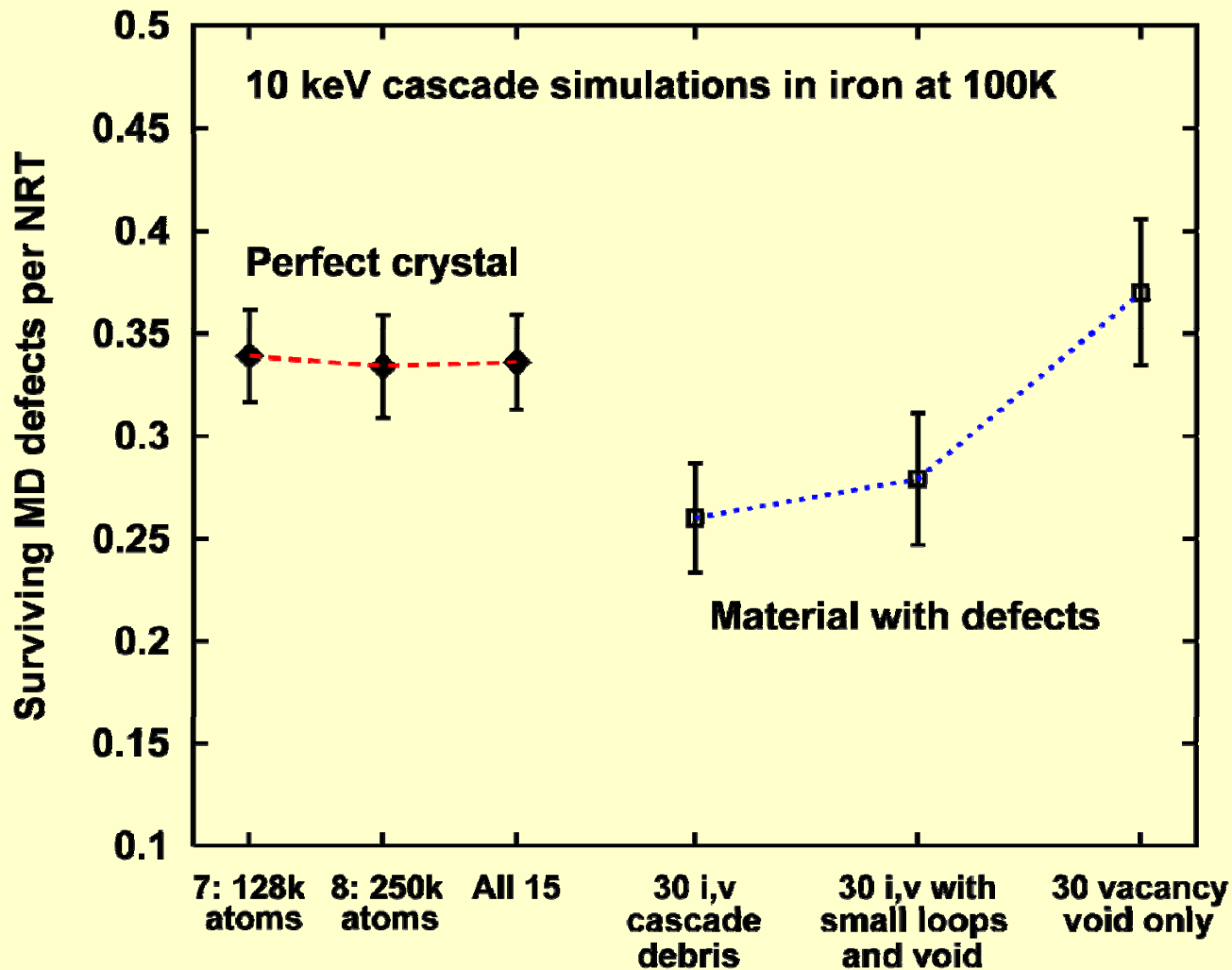# Initial Defect Structures
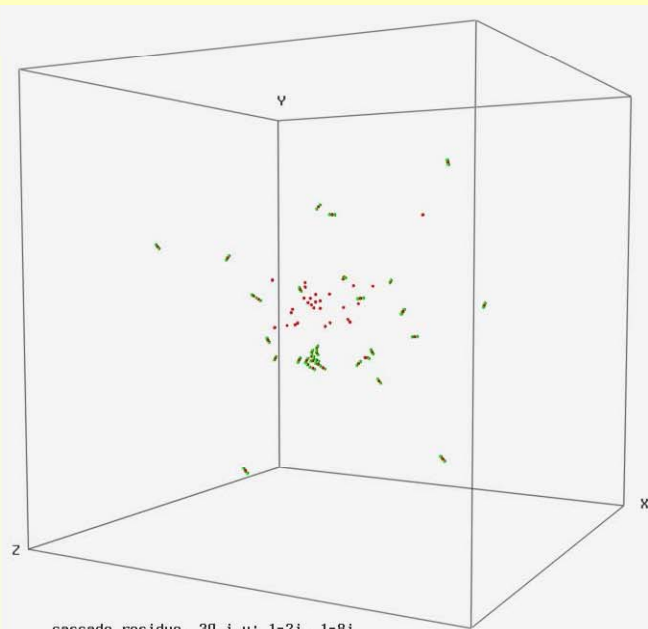
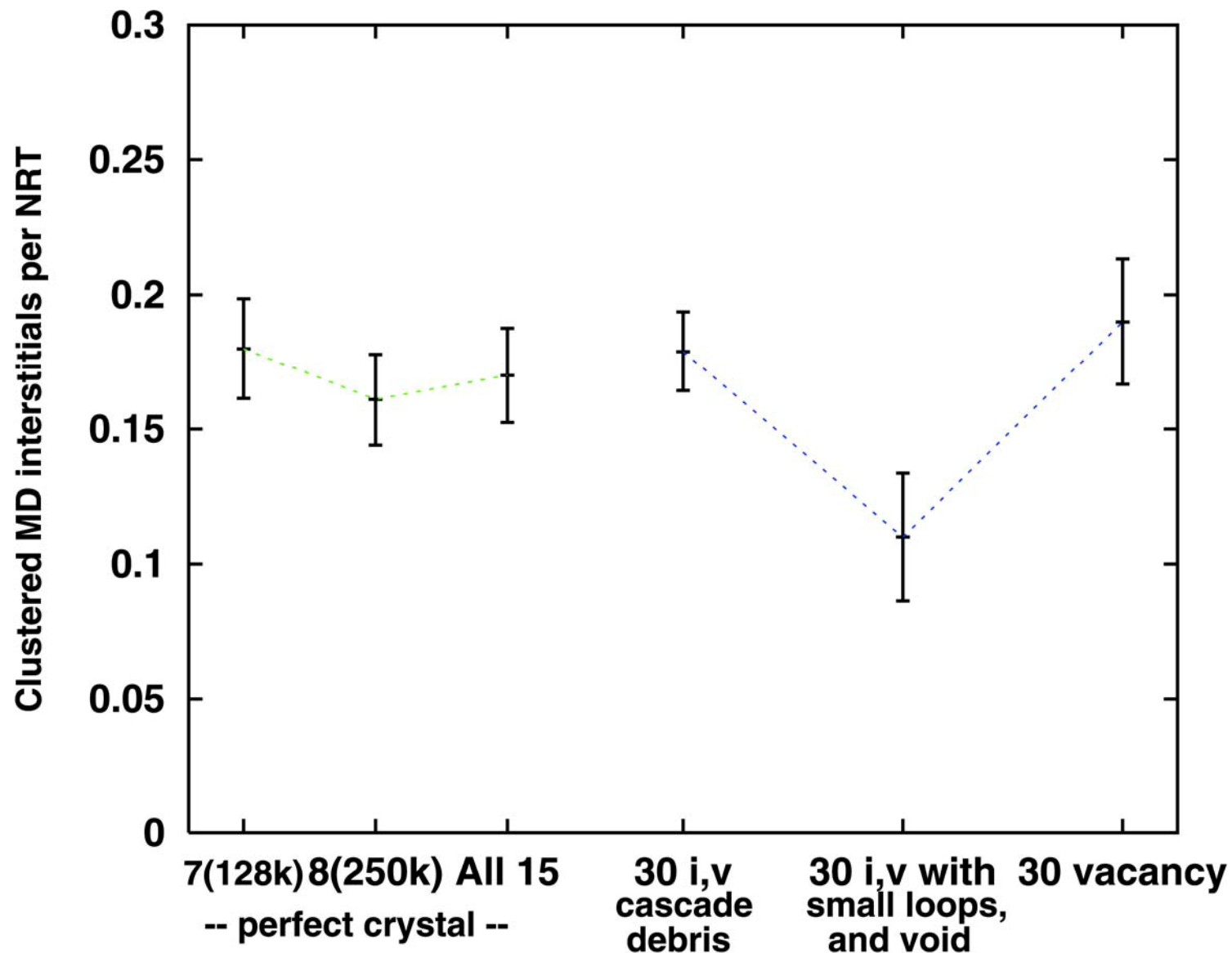cascade residue, 30 i,v: 1-2i, 1-8i
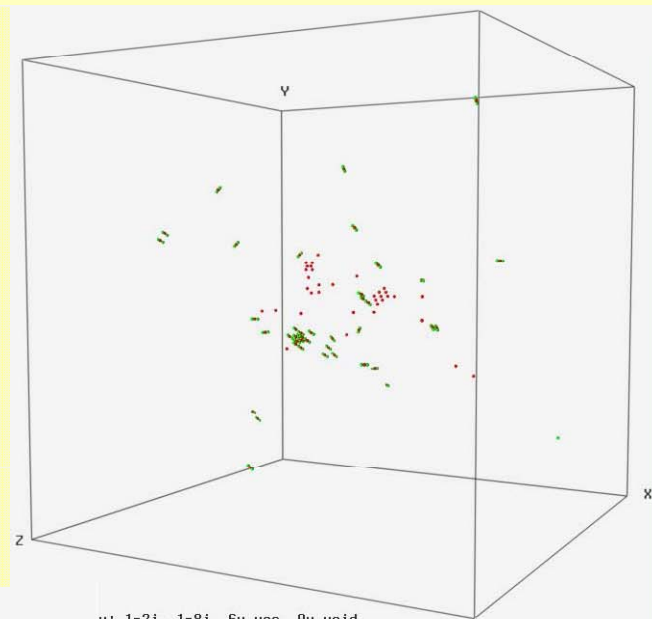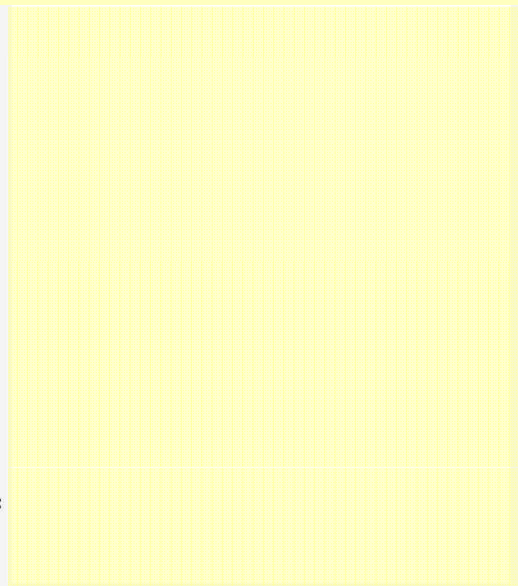
v: 1-2i, 1-8i, 6v vac, 9v void

30 vac void

Pre-existing Damage: Effect on Defect Survival

Pre-existing Damage: Effect on Interstitial Clustering

ornl

Effects of Nearby Free Surface

- Simulations (e.g. Ghaly and Averback in Phys. Rev. Let. 72, 1994; and Nordlund, et al. in Nature 398, 1999) and experimental work (Kiritani in Mat. Sci. For. 15-18, 1987; and Muroga, et al. in Mat. Sci. For. 15-18, 1987) indicates that the presence of a nearby free surface can influence primary damage formation

- Large database on Fe cascades provides opportunity for statistical comparison

- Simulations carried out at 10 and 20 keV using MOLDY with free surface, cascade initiated by surface atom in non-channeling direction

Bulk and surface-initiated cascades 10 keV, 100K
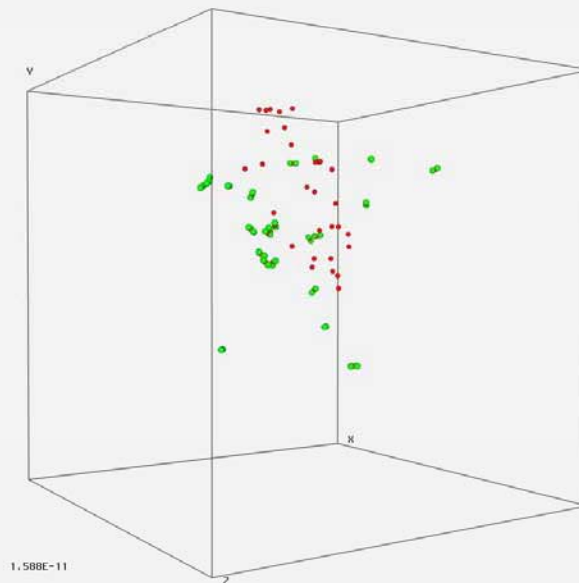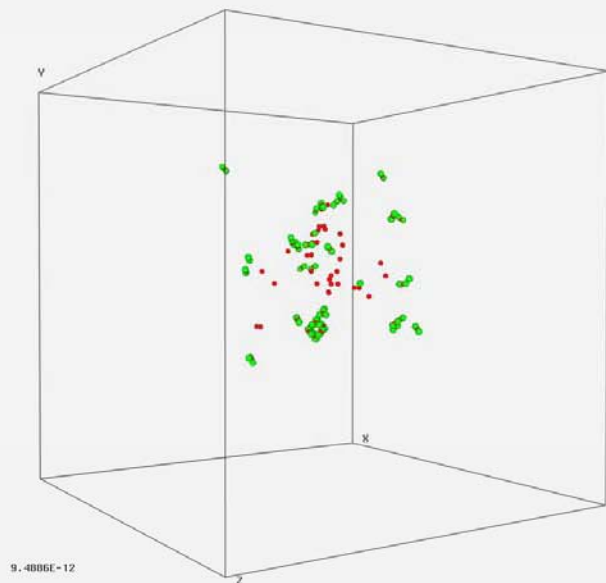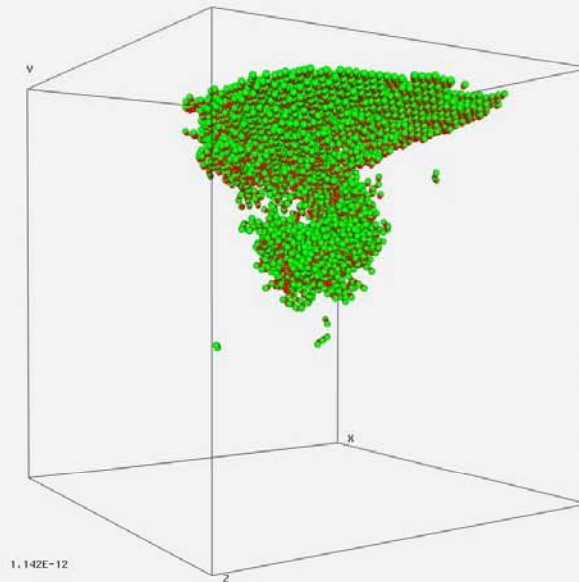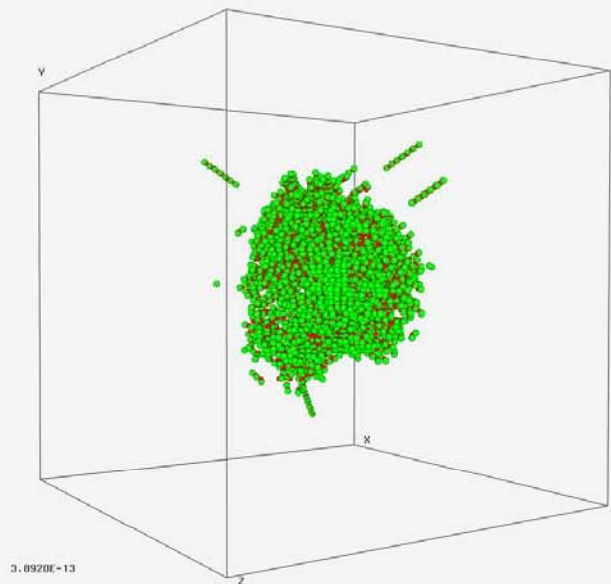
Defect survival in near-surface cascades
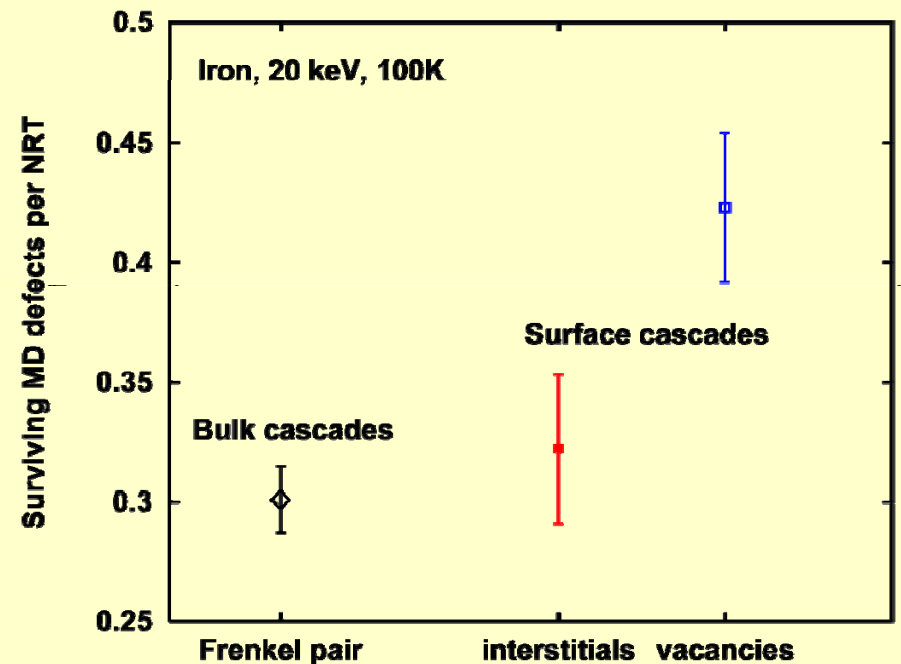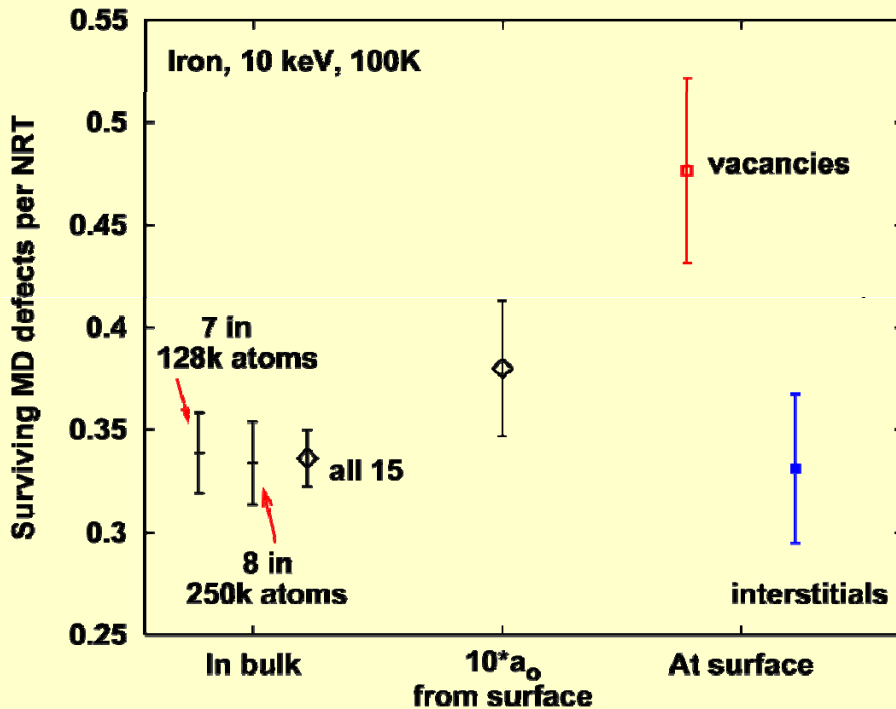
- stable vacancy production increases as cascade initiation site approaches surface
- stable interstitial production may increases or decreases as cascade initiation site approaches surface, effect of energy

Defect clustering in 20 keV near-surface cascades
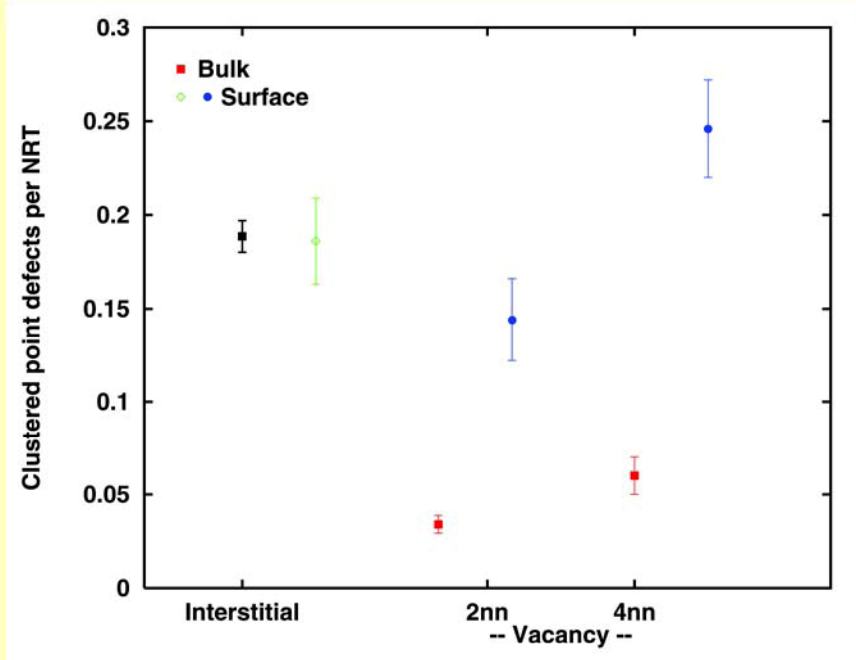
- vacancy clustering increases and cluster sizes increase for near-surface cascades

- only small changes in interstitial clustering for near-surface cascades
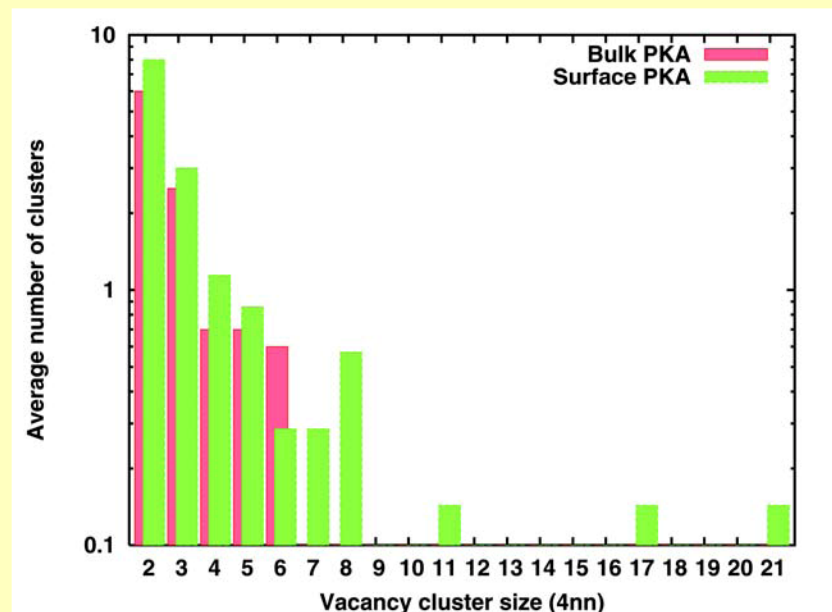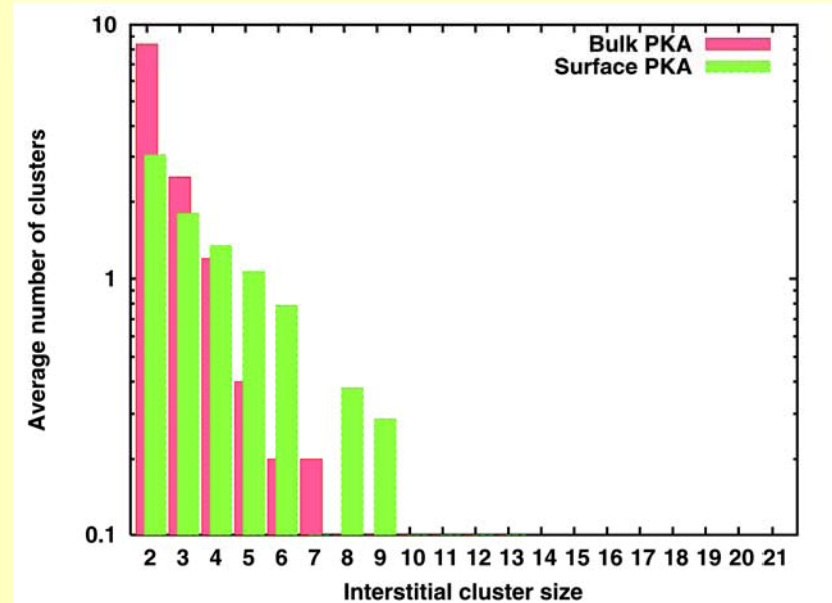
Investigation of potential length-scale effects in primary damage formation

- The MD database provides a good description of primary radiation damage formation from atomic displacement cascades, but most is in perfect, single crystals.

- Large number of mobile defects produced in a displacement cascade, nearby grain boundaries could potentially reduce the residual damage from any given cascade.

- Previous work (e.g. Samaras, et al. in Ni) indicated that the high volume fraction of grain boundaries in bulk nanocrystalline materials could provide efficient point defect sinks and/or recombination sites.

Approach

- Parallel version of MOLDY MD code using OpenMP on shared memory platform

- Voronoi technique used to create nanocrystalline system
  - "Nucleation site" distribution based on an fcc lattice, melted through Monte Carlo using a Lennard-Jones potential

- Choose nanograin "nucleation sites" → Fill in grains → Remove overlapping atoms → Equilibrate structure
  - Nanocrystalline system equilibrated ~200 ps

- Simulate cascade event → Perform nearest neighbor defect analysis → Differentiate grain boundary reconstruction from in-grain defects
  - Cascade simulation was run for ~15 ps, well into the region where the defect count stabilize

Nanocrystalline System: investigate length scale effects on primary damage

- MD simulation cell, 100 lattice parameters (~28.6 nm) on edge, periodic boundaries

- System shown contains 32 grains

- ~10 nm grain size

- Nanocrystalline system equilibrated ~200 ps

- Representative cascade size:

5 keV 🔴   **20 keV** 🟢
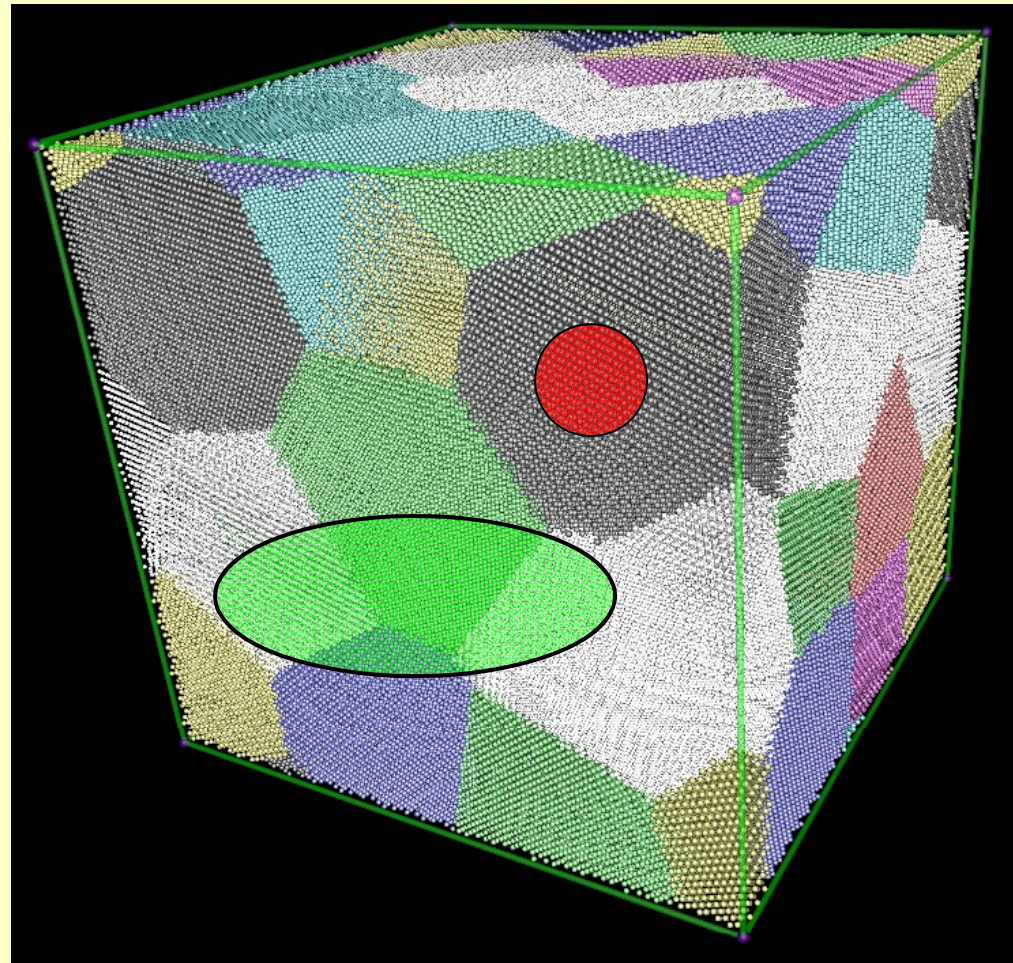
Defect Visualization

- Grain boundaries (GBs) distinguished using spherical approximation – 1st and 2nd nearest neighbor analysis
  - Before and after visualization can show GB movement or reconstruction

- Possible defects flagged when more than 0.3 of a lattice parameter from an original atom site

- Possible in-grain defects flagged when more than 0.5 a lattice parameter from original GBs

Cascade Simulations

- Small study of cascade energy and temperature, 8 simulations at each condition:
  - 10 keV, 100K
  - 20 keV, 100K
  - 20 keV, 600K

- Results compared with "normal" cascade events to determine difference in residual damage between single crystal and nanocrystalline iron cascades

- Previous cascade database for comparison:
  - 10 keV, 100K: 15 events
  - 20 keV, 100K: 10 events
  - 20 keV, 600K: 8 events

Comparison of Final Defect State:10 keV, 100K

Single Crystal Iron

Nanocrystalline Iron
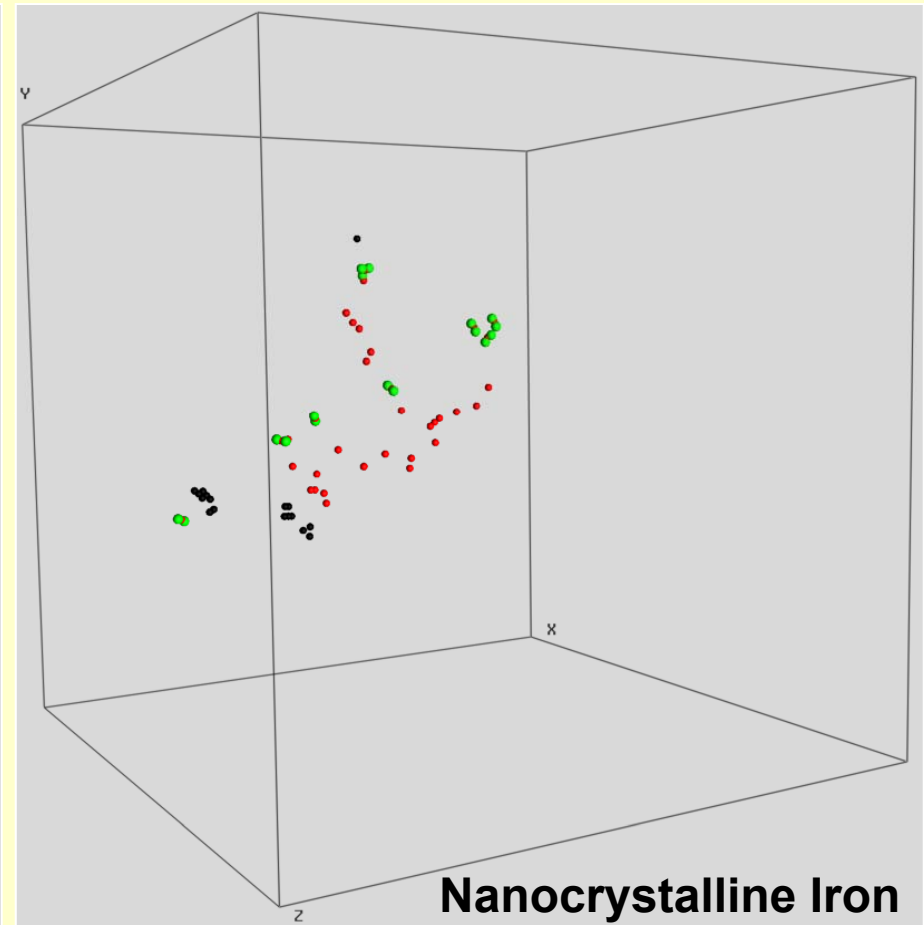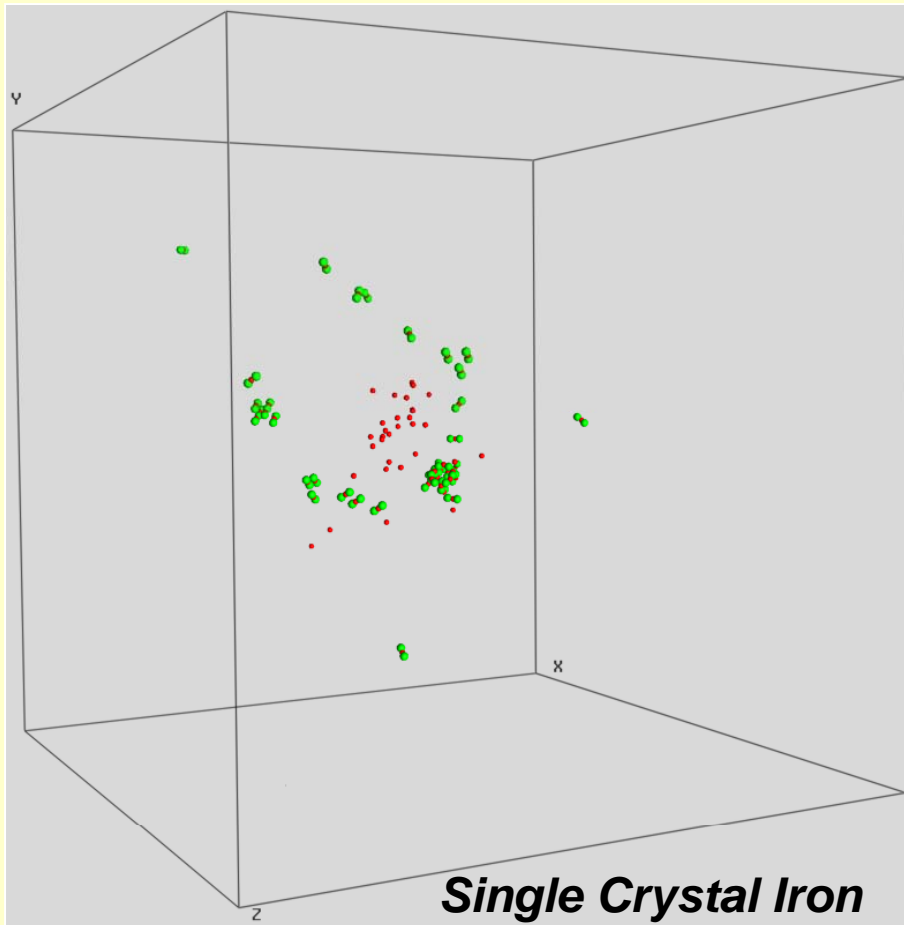
Residual defects - Interstitial atoms are green, vacant sites are red, grain boundary atoms within 3 lattice parameters of any defect are black.

ornl

Comparison with 100 K database
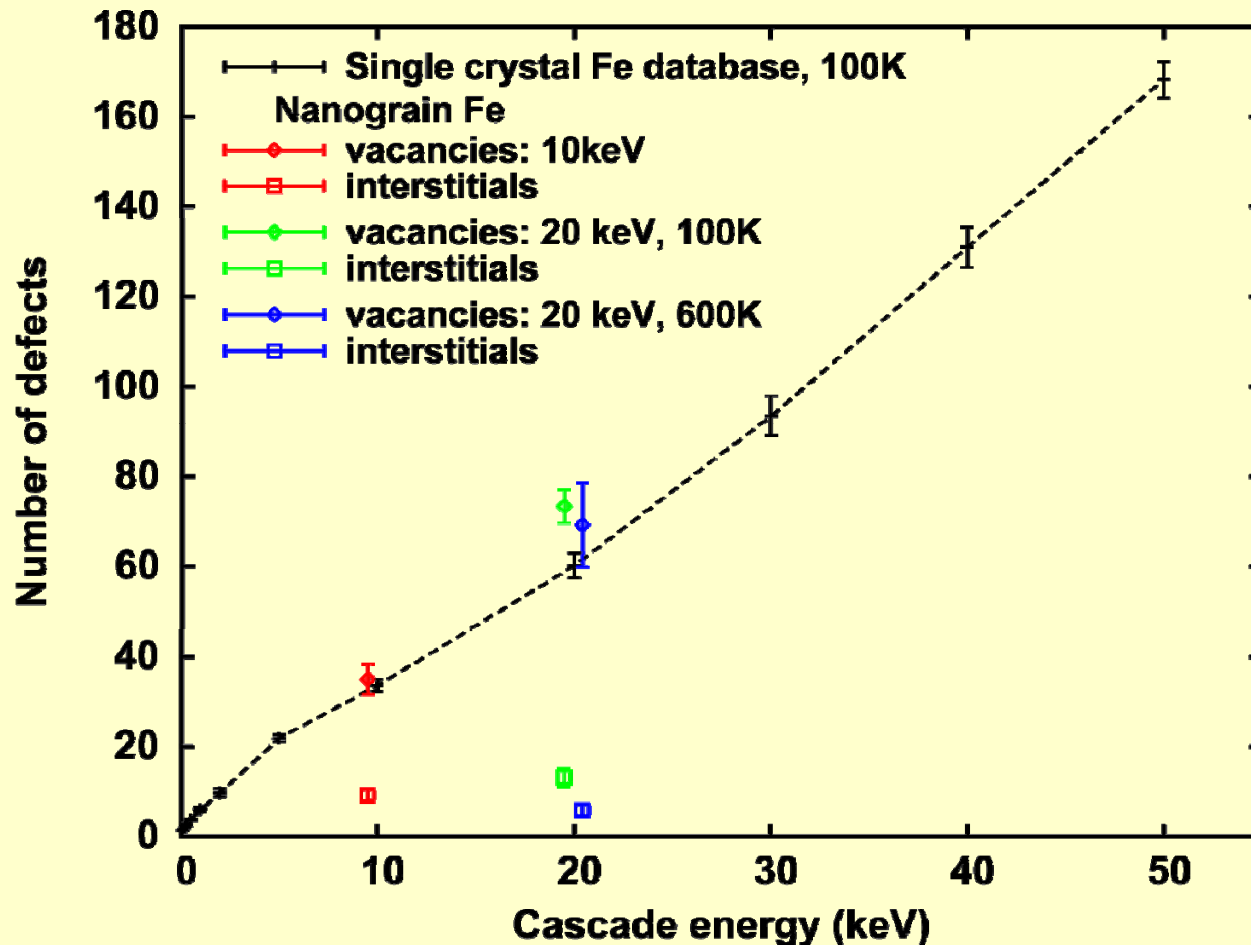
Mean values are shown with the standard error.
- Higher vacancy survival in nanograined material
- Much lower interstitial survival in nanograined material

Results: Stable defect production
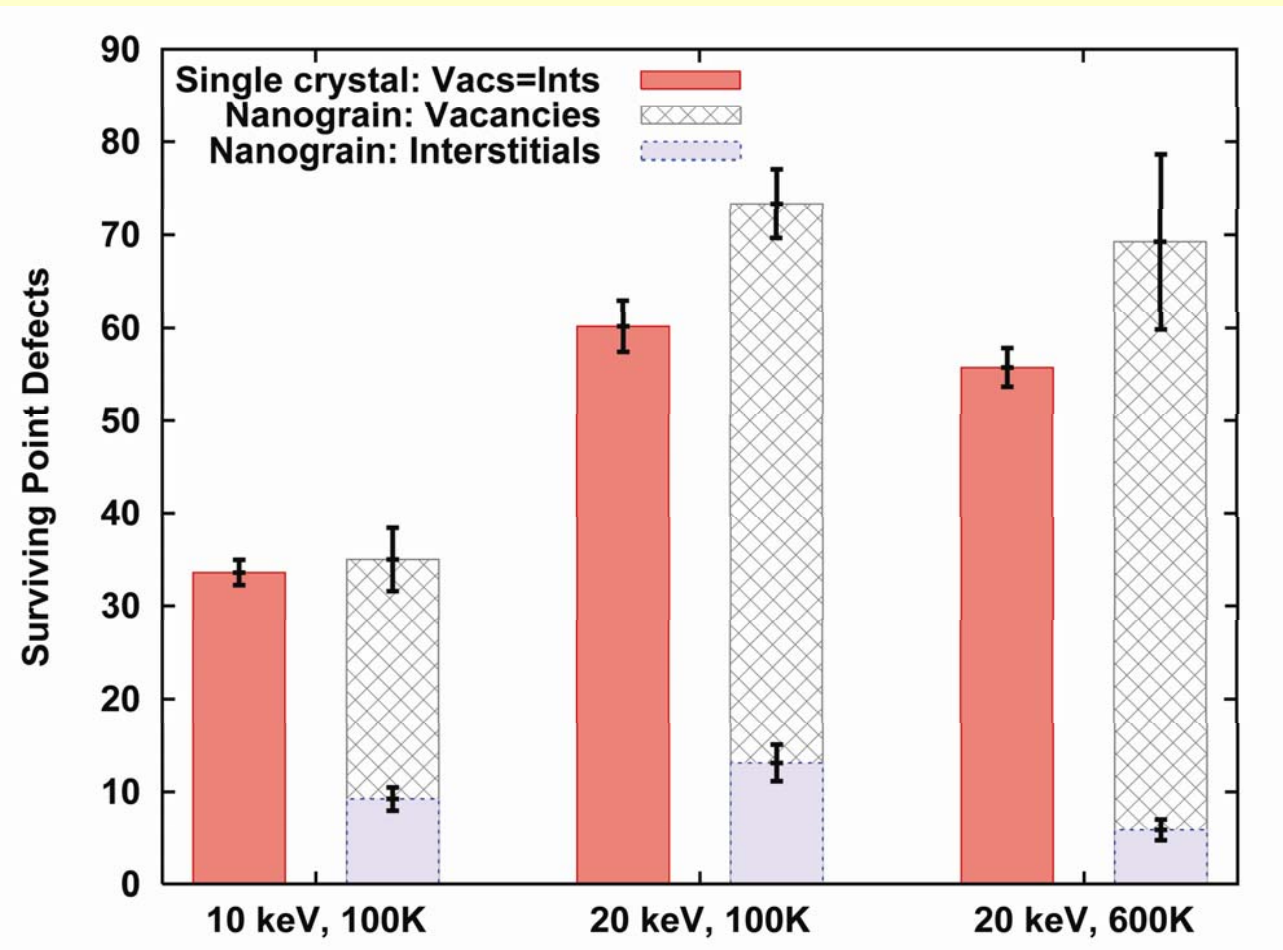
Note: Ni≠Nv

Mean values are shown with the standard error.

- Higher vacancy survival in nanograined material
- Much lower interstitial survival in nanograined material

Results: In-cascade clustering
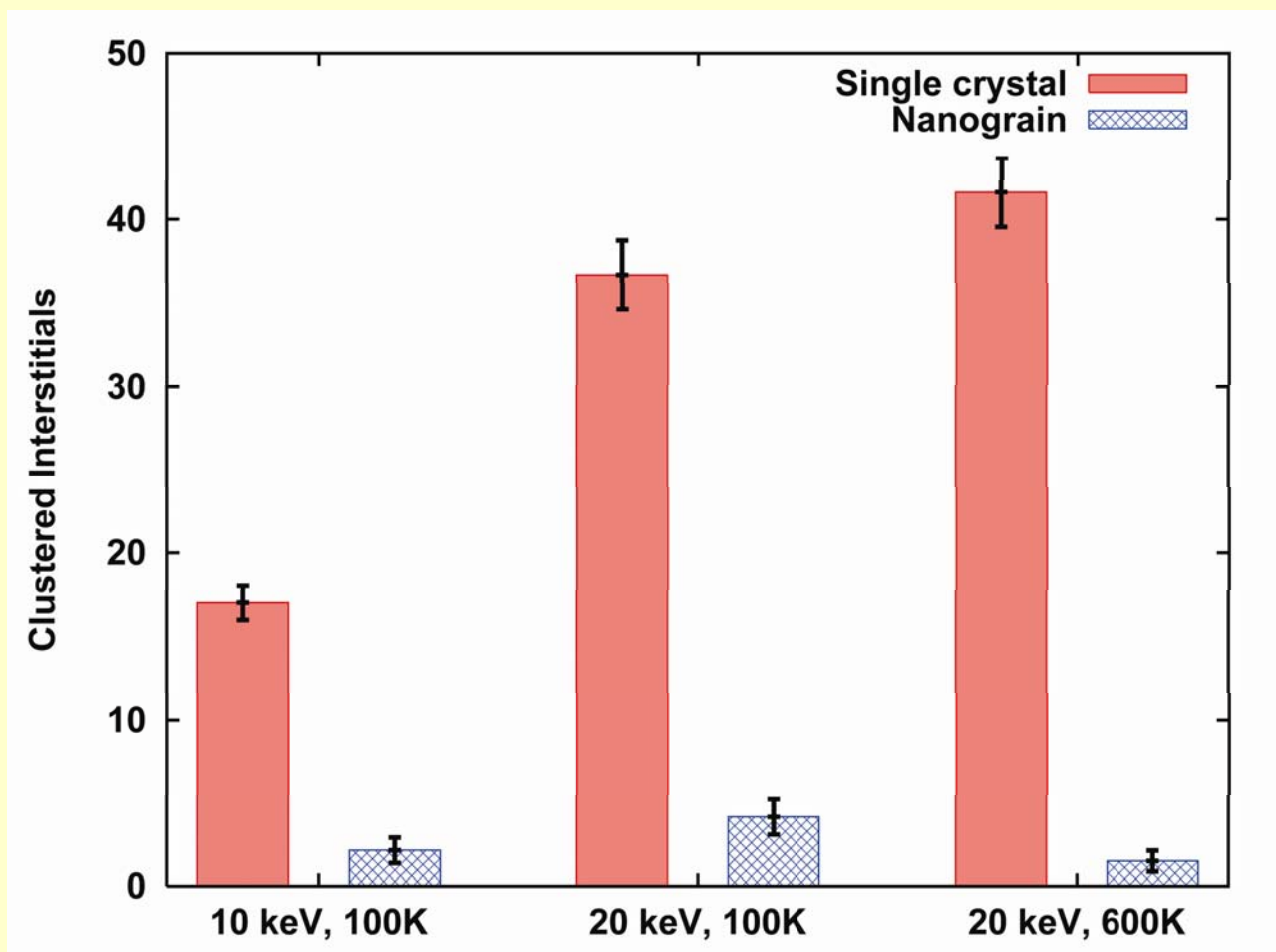
Much less in-cascade interstitial clustering in nanograined material

Summary of cascades in nanograin Fe

- Strong influence of microstructural length scale (grain size) on primary damage production

- Reduced interstitial survival and clustering will reduce formation of radiation-induced microstructural components

- Excess vacancy production may lead to higher supersaturation, greater propensity for cavity formation

- Impact of altered primary damage behavior needs to be evaluated over longer time scale, e.g. using mean field rate theory or Monte Carlo models

- Further analysis of vacancy clustering and grain boundary motion is underway

Effect of Cascade Aging at 600K

- Traditional MD simulation time ~10s of ps, cascade aging not observable

- Previous cascade aging study using kMC (Wirth), showed additional recombination over ~micro-s

- Parallel MD code makes ~ns times practicable

- Preliminary investigation using two disparate 100 keV cascades at 600K

    - very compact cascade, 320 FP survive (32% of NRT), larger interstitial clusters formed - <PKA-9>

    - heavily channeled cascade, more diffuse, 298 FP survive (29.8% of NRT), smaller clusters - <PKA-10>

Use cascade extremes to investigate cascade aging

- **compact: five i-cl$\geq$10 (12 13 14 16 20 40 61), one v-cl$\geq$10 (65)**

- **diffuse: one i-cl$\geq$10 (14), no v-cl$\geq$10**

3.641E-10 s, 53 vacancies
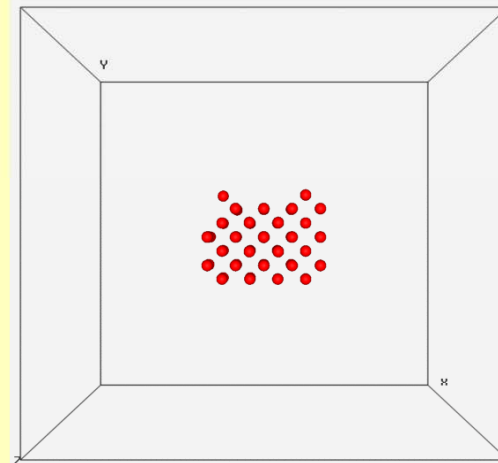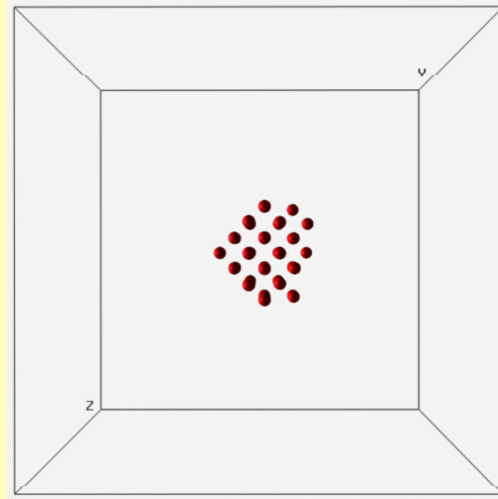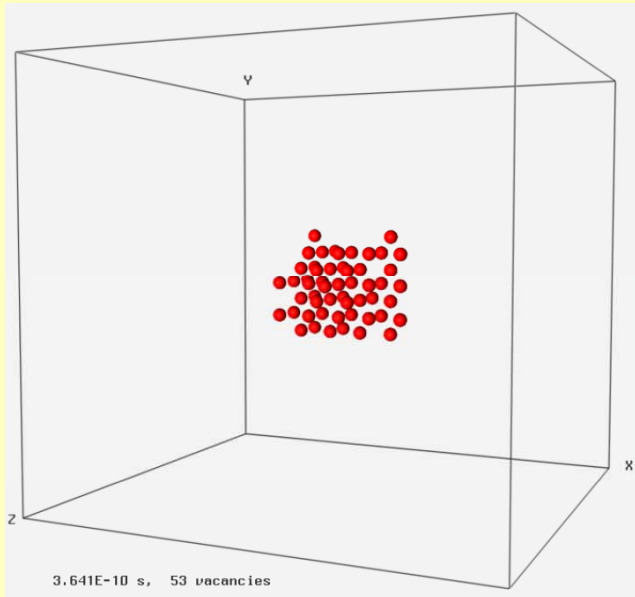
alternate views of ~60 vacancy cluster

Time evolution during cascade aging

- compact: pka-9; diffuse: pka-10

Comparison of MD and MC cascade aging (Wirth, UCB)

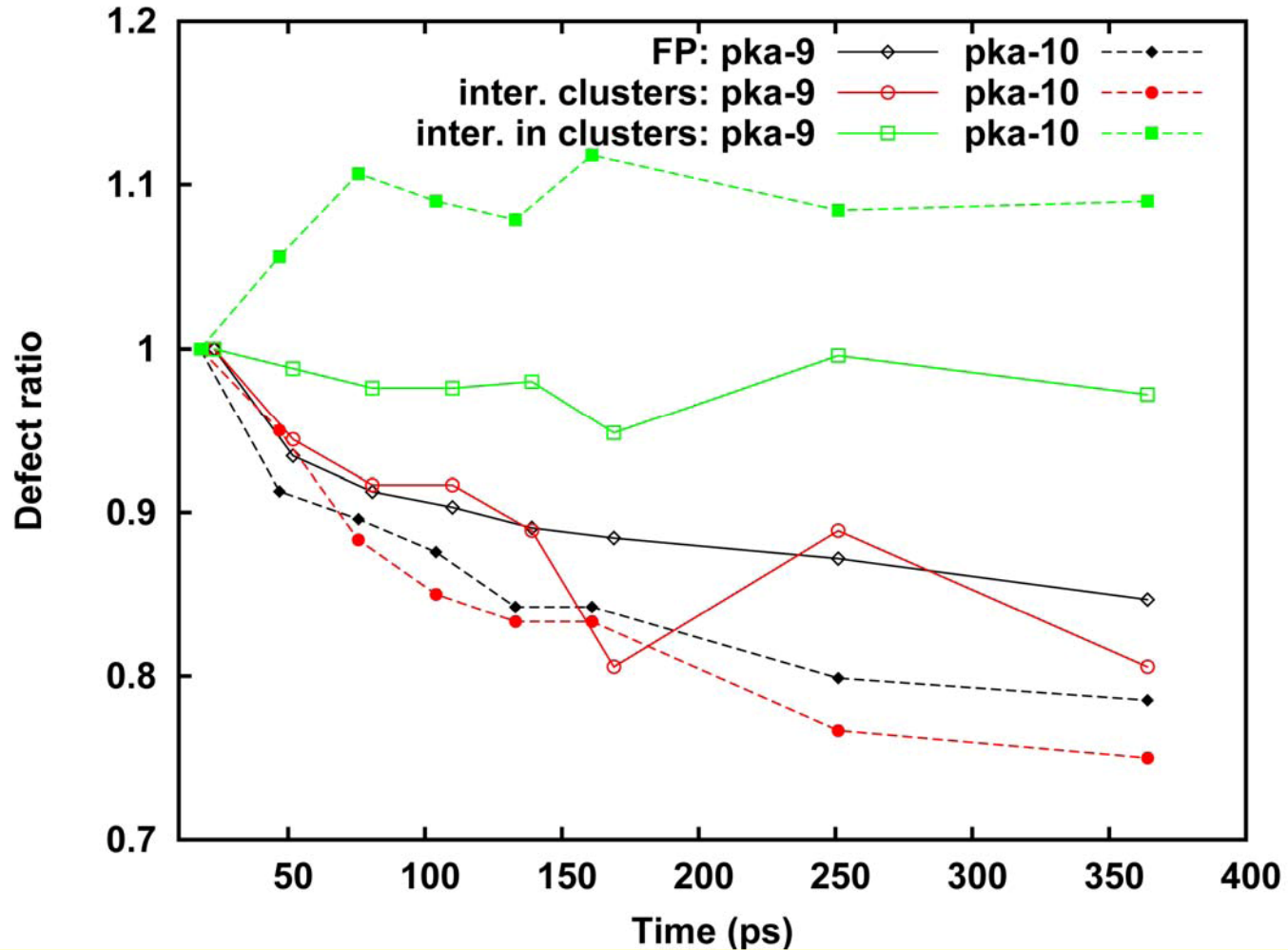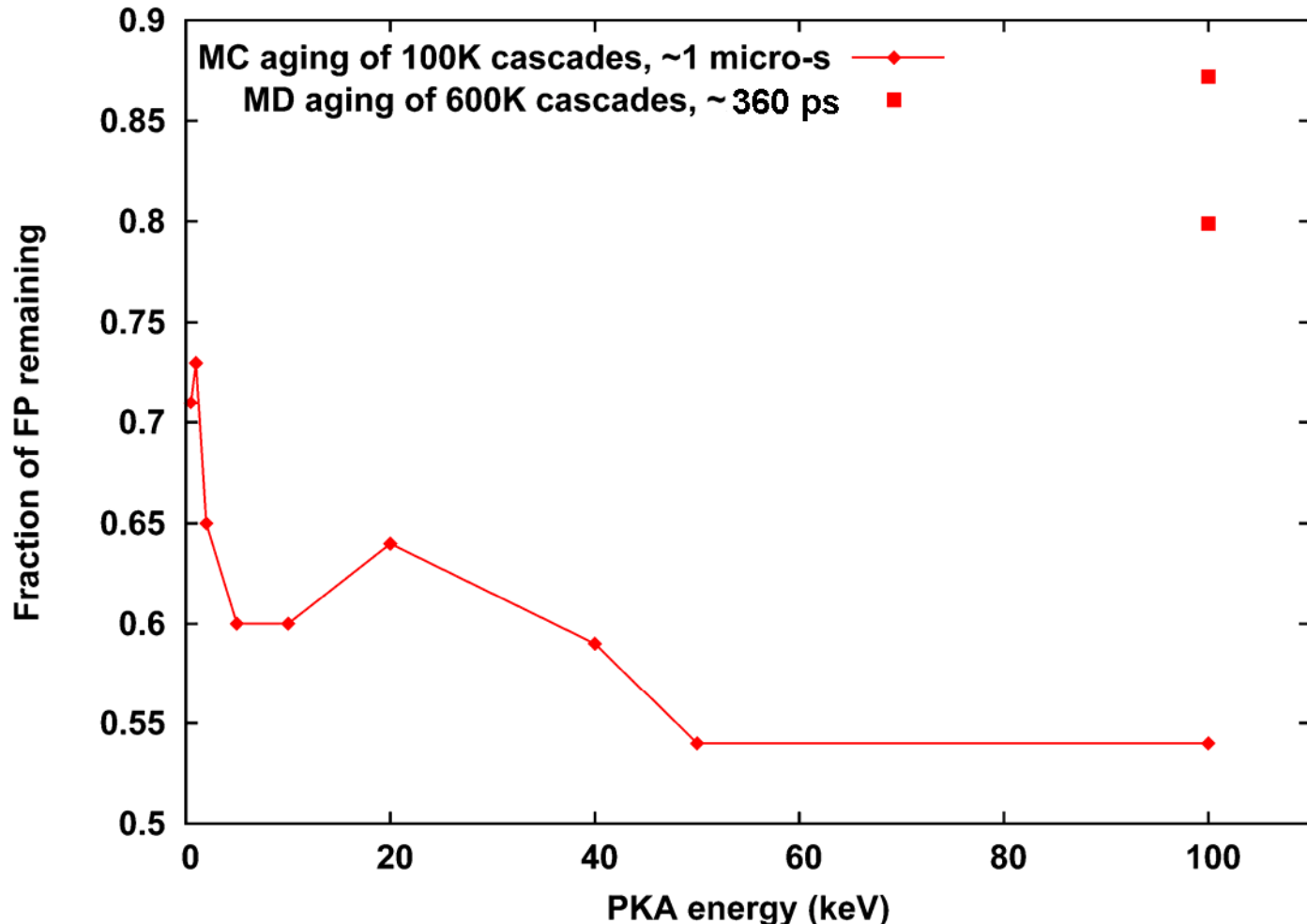# Overall Summary of Primary Radiation Damage

- Cascade energy or PKA energy dependence of stable displacement production is more complex than standard NRT model

- Subcascade formation plays a dominant role in controlling cascade morphology and stable damage production

- Statistical variation needs to be accounted for

  – rare events need to be accounted for: e.g. Soneda, et al. [2001], out of 100 50 keV cascades, one created 50% more stable defects than the average, included a <100> vacancy loop containing 153 vacancies, diameter ~ 2.9 nm

- Clusters formed directly in the cascade account for a substantial fraction of interstitials, many of which are in glissile configurations

  – interstitial clustering fraction and cluster sizes increase with both cascade energy and temperature

  – mesoscale radiation damage models need to be able to account for these clusters, including their rapid 1D mobility

More summary ...

- Significantly less in-cascade vacancy clustering appears, nascent clusters coalesce at longer times, e.g. in KMC simulations of cascade debris

  - vacancy clustering increases with cascade energy and decreases with temperature

- Nearby free surfaces (relevant to in situ experiments), pre-existing damage (cascade overlap) and nanograined microstructure alter defect survival and clustering behavior

Stable defect formation is the result of a series of complex processes involving energetic and coupled many-body reactions

Appendix: dpa and damage correlation

Beginning with the work of Brinkman (1954, 1956), various models were proposed to compute the total number of atoms displaced by a given PKA as a function of energy. The most widely cited model was that of Kinchin and Pease [1955]. Their model assumed that between a specified threshold energy and an upper energy cut-off, there was a linear relationship between the number of Frenkel pair produced and the PKA energy. Below the threshold, no new displacements would be produced. Above the high energy cut-off, it was assumed that the additional energy was dissipated in electronic excitation and ionization.

Later, Lindhard and co-workers developed a detailed theory for energy partitioning that could be used to compute the fraction of the PKA energy that was dissipated in the nuclear system in elastic collisions and in electronic losses [1963]. This work was used by Norgett, Robinson, and Torrens (NRT) to develop a secondary displacement model that is still used as a standard in the nuclear industry and elsewhere to compute atomic displacement rates [1975].

For a good summary, see Olander, "Fundamental Aspects of Nuclear Fuel Elements," 1976

meaning and limitations of dpa

- observed radiation damage depends on some measure of exposure, "damage flux," $\phi > [0.1, 0.5, 1.0]$ MeV, but ions, electrons, photons??

- need to account for differences in PKA energy spectra to be able to correlate data from different types of irradiation

- secondary displacement model by Norgett, Robinson and Torrens, Nucl. Engr. and Des. 33 (1975); based on earlier work by Kinchin and Pease (1955), damage partitioning model by Lindhard, et al. (1963) [see ASTM standards E521 and E693]

- number of displacements, ν_{NRT}, is proportional to fraction of PKA energy that is deposited in elastic collisions, T_{dam}:

$$\nu_{NRT} = \frac{0.8 \cdot T_{dam}}{2 \cdot E_d}$$

- does not account for anything other than total atomic displacements, e.g. no information on in-cascade formation of point defect clusters

- does not account for transmutation production

- does not account for any effects due to ionization

Ratio of damage energy (T_d) to PKA energy (E_{PKA}) as a function of PKA energy \
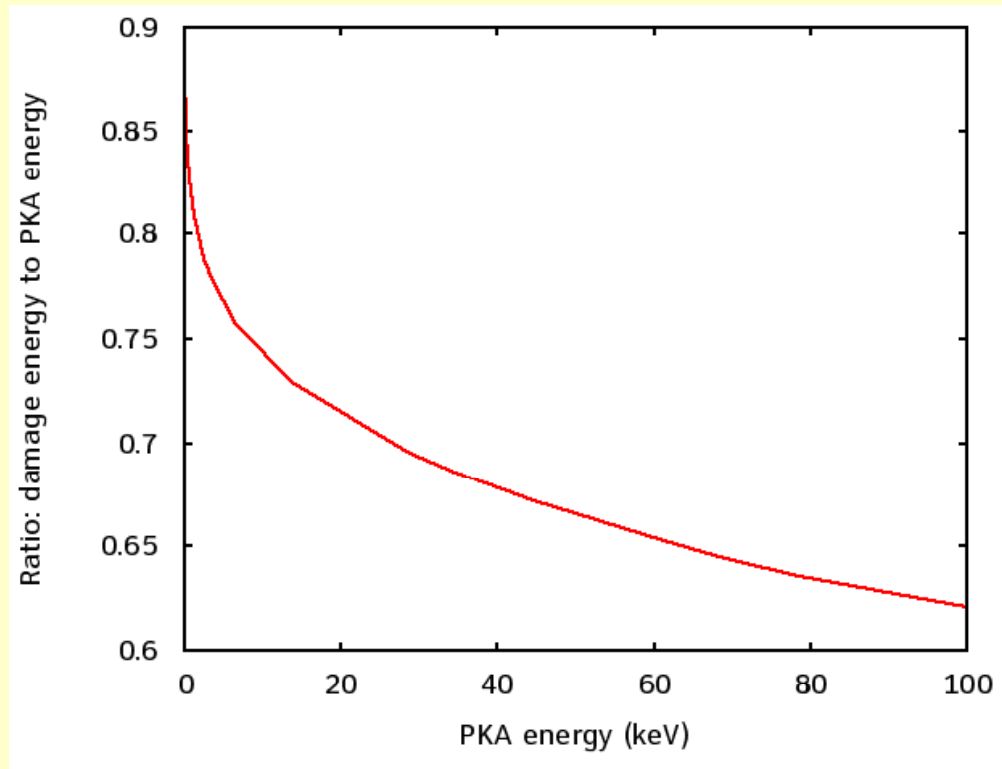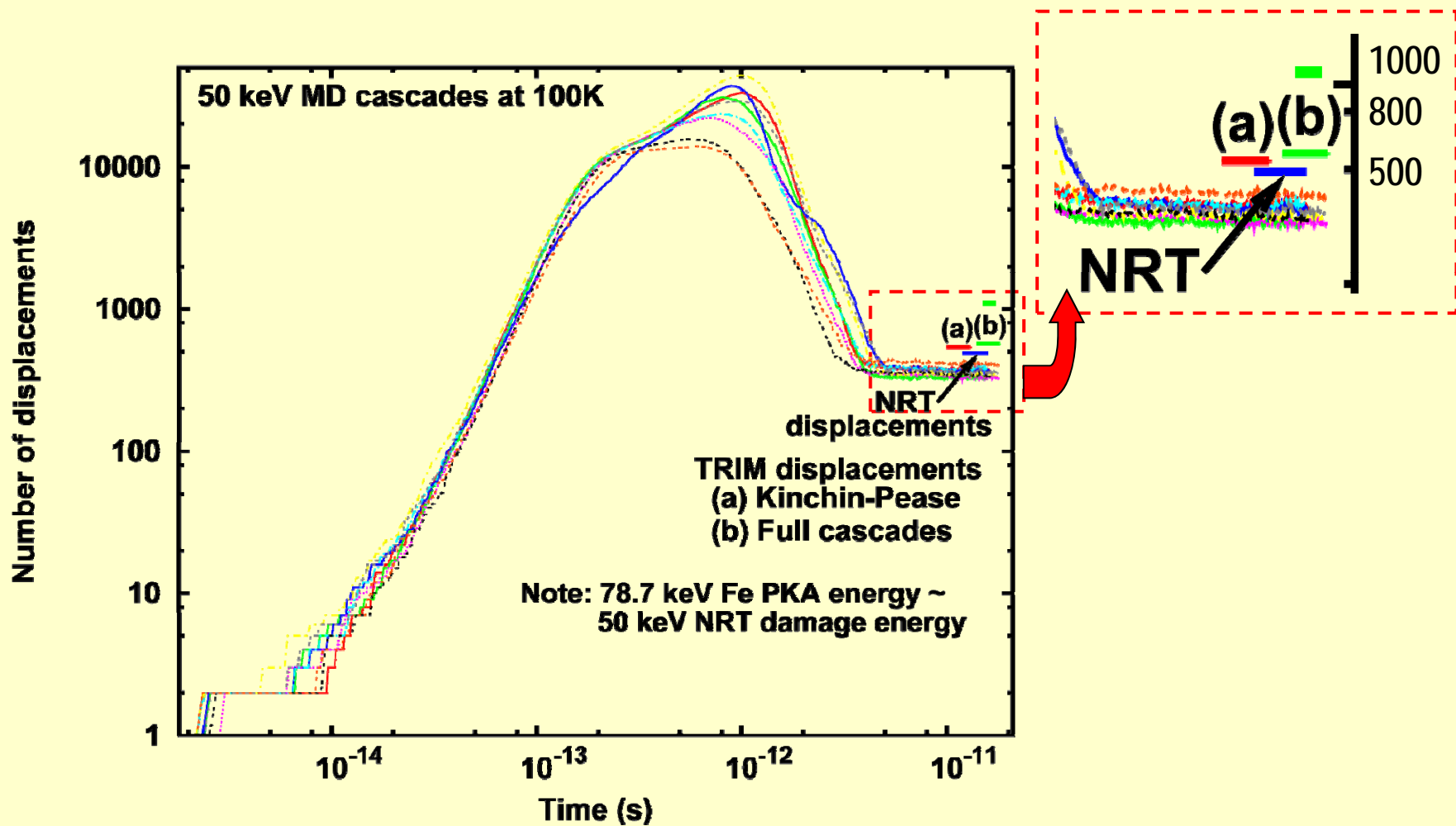

Note that even at low energies a significant fraction of the PKA energy goes into electronic excitation and ionization

Frenkel pair production as a function of PKA energy for Kinchin-Pease and NRT models
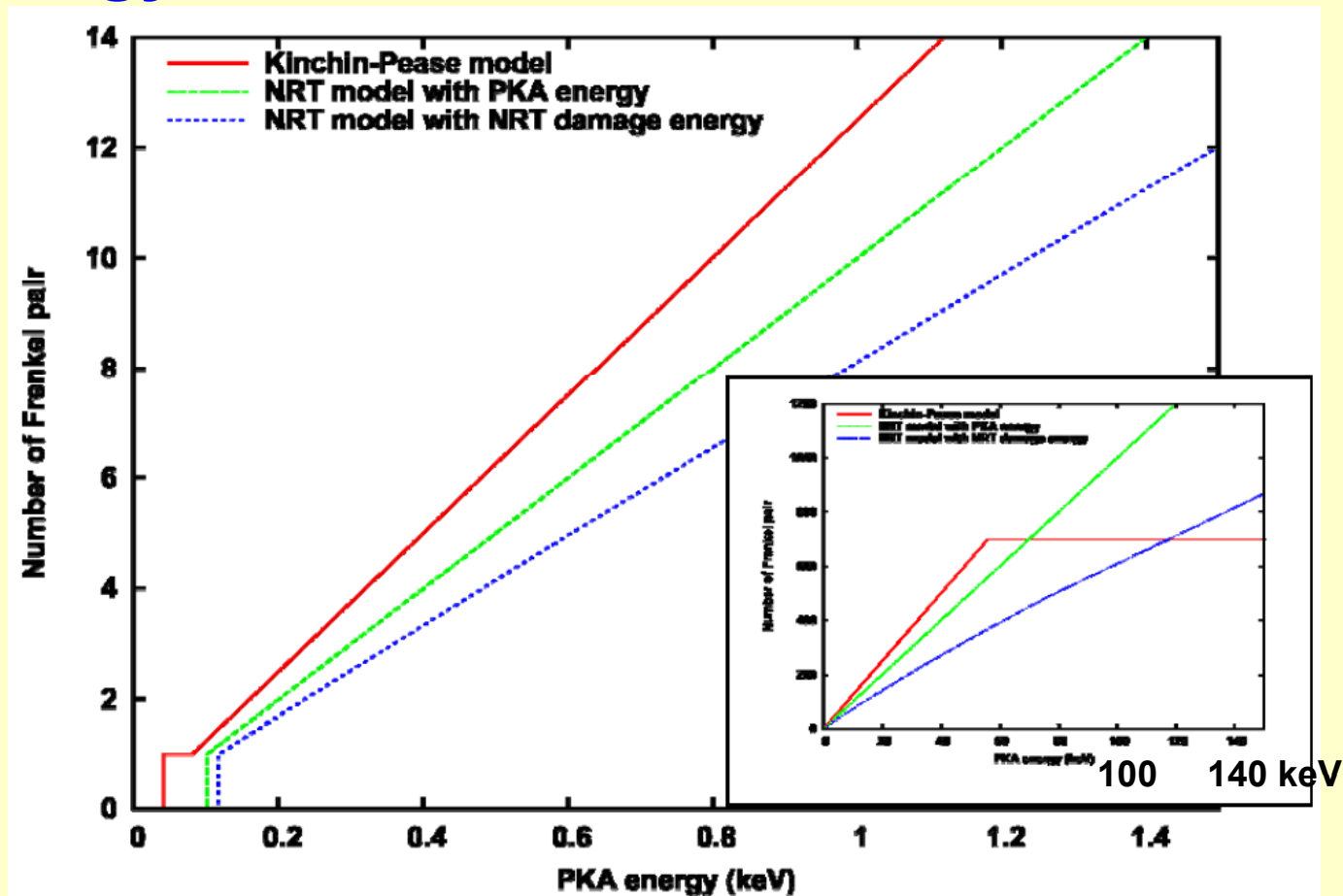
- The inset shows the difference at high energies
- The green curve shows what the NRT model would predict if you (wrongly) used the PKA energy rather than the damage energy

Compare NRT, TRIM, and MD displacements

50 keV MD cascades at 100K

Number of displacements

Time (s)

NRT displacements

TRIM displacements
(a) Kinchin-Pease
(b) Full cascades

Note: 78.7 keV Fe PKA energy ~
50 keV NRT damage energy

NRT

(a)(b)

Number of displacements from TRIM

- varies with method chosen:
  - use integral of output file: vacancy.txt or "Total target vacancies"
  - compute ~damage energy by integrating output files
  - Kinchin-Pease vs. "full cascade" mode
- if reporting dpa for comparison with neutron irradiation
  - use SRIM's "Kinchin-Pease"
  - use standard displacement threshold energy, i.e. 40 eV for iron (see ASTM E521)
  - set lattice and surface binding energy to 0.0

PKA energy (keV)	NRT damage energy (keV)	NRT displacements	Average MD, 100K	TRIM K-P	TRIM Full Cascade
1.0	0.81	8	---	7.7 to 9.4	---
78.7	50	500	168	533 to 540 529*	566 to 572 1052-1075*

* upper row from alternate damage energy integrations, lower row from vacancy.txt

Example of dpa usage in damage correlation

- High Flux Isotope Reactor at ORNL, ~1986 - an unwelcome technical surprise

- potential explanations:
  - material sensitivity, misapplication of original database
  - rate (flux) effect
  - spectrum effect
  - transmutation effect

- extended outage, much analysis, many $$ later
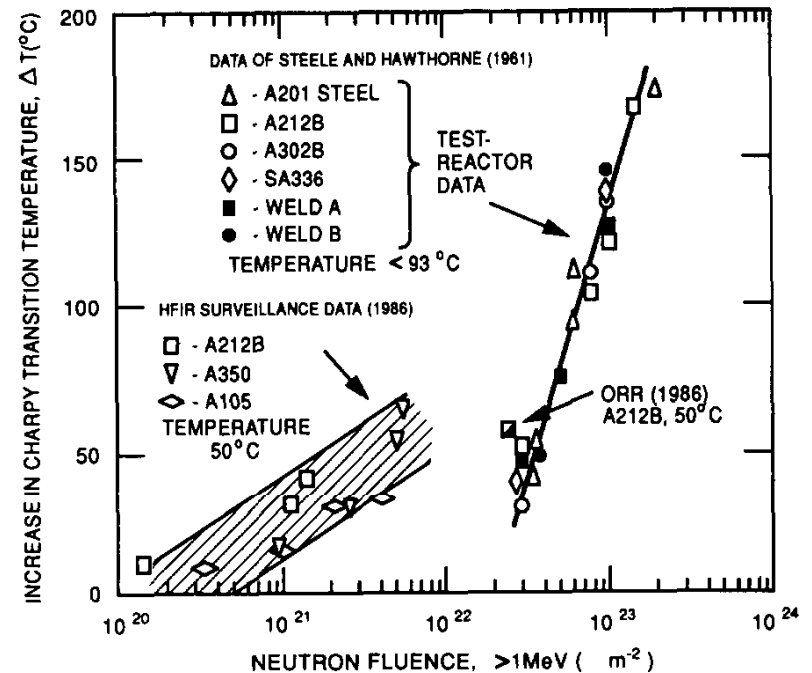 - incomplete dosimetry
  - poor damage correlation

Fig. 1. Comparison of HFIR surveillance and ORR data with test reactor irradiations of similar materials at temperatures < 93°C.

Figures from Remec, et al., J. Nucl. Mat. (1994)]

Partial sequence of events

- additional irradiation experiment in ORR using HFIR archive material, confirmed accelerated embrittlement

- recalculation of neutron fluxes, little change

- correlate with dpa (neutron) rather than fluence > 1.0 MeV, little change
  - initial attention on thermal flux in "Key 7" position due to coarse grouping scheme and cross section set used to compute fast flux, later reduced by ~10

- dosimetry experiments generally confirmed new calculations, except:
  - for [237]Np fission monitor and Be helium accumulation monitor
  - indicated fast flux ~15 times higher than Ni monitor
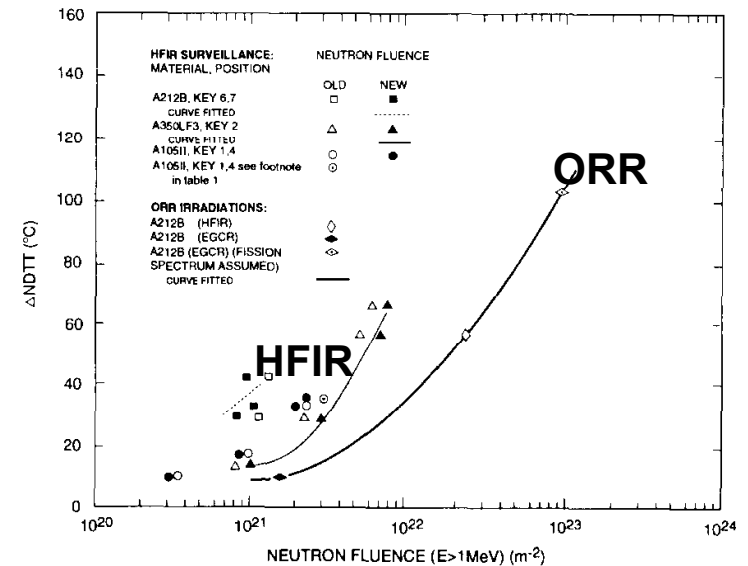

Fig. 4. Charpy NDTT shifts versus fast neutron fluence for HFIR surveillance materials irradiated in HFIR and in ORR.
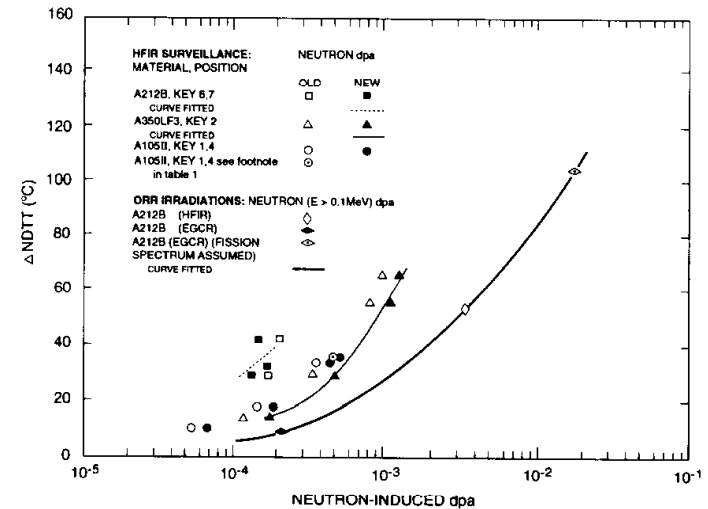

Fig. 5. Charpy NDTT shifts versus dpa for HFIR surveillance materials for neutron-induced dpa from new analysis (all energies) and old analysis (> 0.1 MeV), and in ORR for neutron-induced dpa ($E > 0.1$ MeV).

- results from Np and Be ultimately explained by photon-induced reactions
- HFIR geometry lead to anomalous high ratio of hard gamma rays to fast neutrons near RPV
  - Be reflector
  - substantial water between core
- Charpy shift well correlated on the basis of total, (neutron + γ) generated dpa - HFIR/ORR and original test reactor database

  ———————

- Jones, et al. ASTM STP 1366 (2000), had similar success with dpa when correlating damage in MAGNOX reactor steels, high thermal-to-fast neutron flux ratio
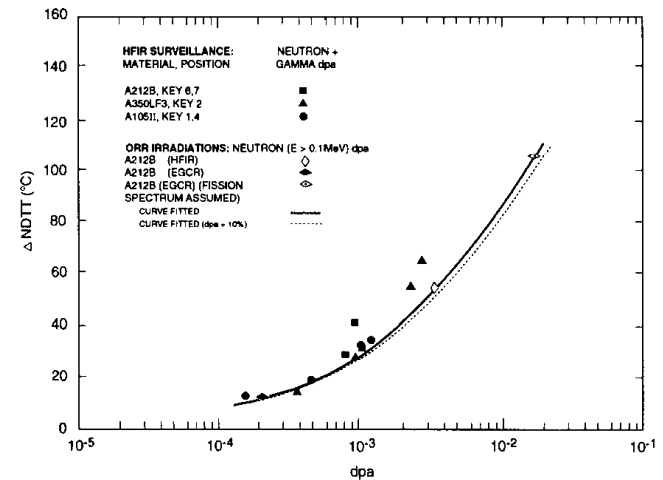

Fig. 6. Charpy NDTT shifts versus dpa for HFIR surveillance materials for neutron-induced and gamma-induced displacements (all energies) and in ORR for neutron-induced displacements ($E > 0.1$ MeV).
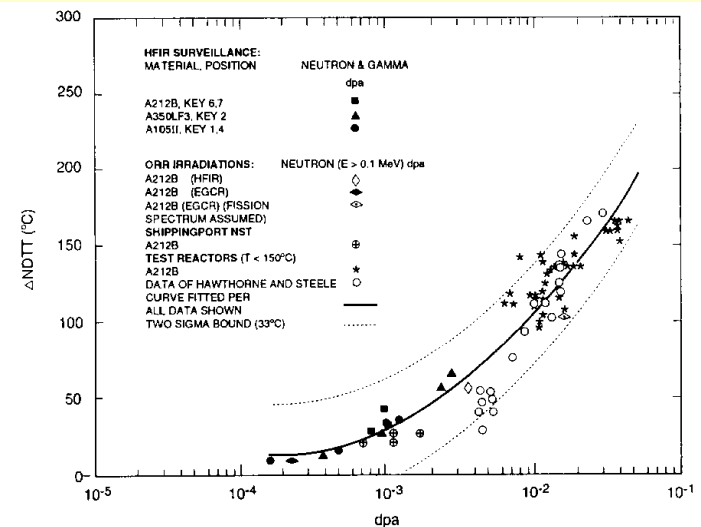

Fig. 8. Comparison of Charpy NDTT shifts versus dpa for HFIR surveillance materials for neutron-induced and gamma-induced displacements (all energies), and the data points of Steele and Hawthorne [28], ORR, other test reactors and Shippingport NST for neutron-induced displacements ($E > 0.1$ MeV).